Active-RIS Enhances the Multi-User Rate of Multi-Carrier Communications

H. D. Tuan[1], A. A. Nasir[2], E. Dutkiewicz[1], H. V. Poor[3], and L. Hanzo[4]

***Abstract*—This paper explores a multi-user multi-carrier system leveraging an active reconfigurable intelligent surface (RIS), where the joint design of the RIS's programmable reflecting elements and the subcarrier-wise beamformers at the base station is investigated. To overcome the limitation of the conventional design, which aims solely at sum-rate maximization resulting in zero rates for some users across all sub-carriers and thus failing to boost all users rates, we propose the two alternative designs: one maximizing the geometric mean of the users' rates (GM-rate maximization) and the other maximizing the soft users' minimum rate (soft max-min rate optimization). However, they pose challenges as large-scale nonconvex problems, rendering convex-solver computational approaches impractical. To tackle this, we develop iterative computational procedures based on closed-form expressions of scalable complexity. Extensive simulations demonstrate the substantial benefits of these novel designs in significantly enhancing multi-user rates. Notably, under the same power budget, the active-RIS-assisted multi-carrier system achieves approximately twice the minimum user-rate or sum rate compared to RIS-less or passive-RIS-assisted counterparts.**

***Index Terms*—Active reconfigurable intelligent surface, multi-carrier communication, subcarrier-wise beamforming, multi-user rate enhancement, large-scale computation**

I. Introduction

Reconfigurable intelligent surfaces (RISs) have shown great promise in enhancing the performance of future wireless communication networks by enabling the controlled reflection of incident waves in desired directions [1]–[3]. To date, passive RISs with programmable reflecting elements (PREs) have been extensively studied owing to their low power consumption [4]–[12]. However, the signals reflected by passive RISs encounter double path loss (multiplicative fading) and experience notable attenuation [13], thereby limiting their overall impact. The concept of an active-RIS, which facilitates power amplification of incident signals, has been introduced in [14], [15] to to address this double path-loss phenomenon. Previous studies [15]–[17] have explored the joint design of transmit multi-user beamformers and the active RISs PREs to maximize the multi-user (MU) sum-rate (SR).

The employment of multi-carrier (MC) communication based on orthogonal frequency division multiplexing (OFDM) techniques to combat frequency-selective multi-path propagation is crucial for meeting the demands of high-data-rate applications [18]. Considering passive-RIS aided MC communication, recent papers have considered the design of the PREs for RIS-assisted single-user OFDM [19]–[22], for orthogonal frequency division multiple access (OFDMA) [23]–[26], and for MU OFDM [27], [28]. In particular, the authors of [27] addressed such joint design to maximize the SR. However, as observed in [29], maximizing the SR leads to zero rates across all frequency bands for certain users, failing to enhance rates for all users and thus is unsuitable for MU OFDM. Max-min rate optimization, which aims to maximize the users' minimum rate (MR), is a systematic approach for enhancing MU rates. However, it involves a nonsmooth optimization problem that is computationally challenging [28]. Building on the approaches to enhance MU rates in single-carrier scenarios [10], [11], the work [28] has proposed an approach to enhance MU rates in MC scenarios by maximizing the geometric mean of users rates (GM-rate). Leveraging the smoothness of the GM-rate objective, GM-rate maximization facilitates tractable computation through iterating closed-form expressions of scalable complexity. The joint design of the PREs and transmit beamformers for active RIS-assisted MC communication was recently considered in [30], aiming to maximize the SR. Beside failing to enhance all users rates, the computation method in [30] suffers from impractical computational complexity. For instance, in a scenario of 64 subcarries, 10 transmit antennas, and 10 users, the method in [30] necessitates iterating convex problems of $64 \times 10 \times 10 = 6400$ decision variables for subcarrier-wise beamforming alternating optimization.

Against the above background, this paper presents the first comprehensive investigation into the potential of an *active-RIS-assisted MC communication system* conceived for delivering high rates to all users. By contrast, when the sum-rate of a system is optimized, typically the users having high channel-quality are granted a high rate while some others might have near-zero rate. The contributions of this paper can be summarized as follows:

- We present a joint design of the active-RIS PREs and of the MU transmit beamformers at the base station (BS) to maximize the GM-rate. We develop a computational solution that iteratively improves both the PREs and MU beamformers using closed-form expressions. Notably,

This work was supported in part by the Australian Research Council's Discovery Projects under Grant DP190102501, in part by the Deanship of Research Oversight and Coordination (DROC) at KFUPM for funding under the Interdisciplinary Research Center for Communication Systems and Sensing through project No. INCS2403, in part by the U.S National Science Foundation under Grants CNS-2128448 and ECCS-2335876, and in part by the Engineering and Physical Sciences Research Council projects EP/W016605/1, EP/X01228X/1, EP/Y026721/1 and EP/W032635/1 as well as of the European Research Council's Advanced Fellow Grant QuantCom (Grant No. 789028)

[1]School of Electrical and Data Engineering, University of Technology Sydney, Broadway, NSW 2007, Australia (email: tuan.hoang@uts.edu.au, eryk.dutkiewicz@uts.edu.au); [2]Department of Electrical Engineering and Center for Communication Systems and Sensing, King Fahd University of Petroleum and Minerals, Dhahran 31261, Saudi Arabia (email: anasir@kfupm.edu.sa); [3]The department of Electrical and Computer Engineering, Princeton University, Princeton, NJ 08544, USA (email: poor@princeton.edu). [4]School of Electronics and Computer Science, University of Southampton, Southampton, SO17 1BJ, U.K. (e-mail: lh@ecs.soton.ac.uk).

these iterations are computationally tractable even for large-scale networks.

- We also propose another optimization problem, referred to as "soft max-min (SMM) rate optimization," which is based on a smooth and approximate lower bound of the non-smooth MR function. We develop a computational solution for this problem relying on the iterative evaluation of closed-form expressions. Our simulation results demonstrate that the SMM-rate optimization further improves both the MR and SR, when it is initialized by the solution gleaned from GM-rate maximization.
- Our simulations demonstrate that the active-RIS-assisted MU MC system conceived achieves approximately twice the MR or SR compared to the RIS-less or passive-RIS-assisted MU MC system, given the same total power-budget. We also observe that conventional SR maximization is not suitable for active-RIS-assisted MU OFDM, as it results in near-zero rates for certain users. By contrast, both GM-rate and SMM-rate optimizations effectively address this issue while maintaining a good SR. More particularly, SMM-rate optimization closely matches the SR provided by SR maximization, especially at higher total power budgets or with a larger number of transmit antennas at the BS.

In conclusion, Table I provides a concise and comprehensive comparison of our novel contributions to the literature.

The paper is organized as follows. Section II presents the system model and problem statement. Sections III and IV propose closed-form expression-based algorithms of scalable complexity for solving the GM-rate and SMM-rate optimization problems, respectively. Our simulation results are discussed in Section V, followed by our conclusions in Section VI.

Notation. Boldfaced letters are used for decision variables; I_N is the identity matrix of size $N \times N$. For $x = (x_1, \ldots, x_n)^T$, $\mathsf{diag}(x)$ represents a diagonal matrix of the size $n \times n$ with $x_1, \ldots, x_n$ on its diagonal. The notation $\|x\|$ denotes the Euclidean norm of the vector x. The notation $X \succeq 0$ ($X \succ 0$, resp.) for the Hermitian symmetric matrix X means that it is positive semi-definite (positive definite, resp.). Lastly, F_S is the fast Fourier transform (FFT) matrix of order S defined as

$$F_S \triangleq \frac{1}{\sqrt{S}}[e^{-\jmath 2\pi kp/S}]_{k,p=0,1,\ldots,S-1}$$

Note that F_S is unitary $F_S F_S^H = I_S$ so F_S^H is called the inverse FFT (IFFT) matrix. Table II provides a summary of the basic notations used in the paper.

Tight minorant maximization and tight majorant minimization as key ingredients. For all $\mathbf{v} \in \mathbb{C}$, $\mathbf{y} > 0$, and $\bar{v} \in \mathbb{C}$, $\bar{y} > 0$, the following inequality holds [33]:

$$\ln\left(1+\frac{|\mathbf{v}|^2}{\mathbf{y}}\right) \geq \ln\left(1+\frac{|\bar{v}|^2}{\bar{y}}\right) - \frac{|\bar{v}|^2}{\bar{y}} + 2\frac{\Re\{\bar{v}^*\mathbf{v}\}}{\bar{y}} - \frac{|\bar{v}|^2}{\bar{y}(|\bar{v}|^2+\bar{y})}(|\mathbf{v}|^2+\mathbf{y}). \quad (1)$$

The right-hand side (RHS) of (1) matches its left-hand side (LHS) at $(\mathbf{v}, \mathbf{y}) = (\bar{v}, \bar{y})$, so the former provides a tight minorant of the latter [34]. As such maximizing the former, called tight minorant maximization, helps to generate a better point than $(\bar{v}, \bar{y})$ for the latter.

Over the domain $\mathrm{dom} \triangleq \{(\boldsymbol{x}_k, \mathbf{y}_k) \in \mathbb{C} \times \mathbb{R} : \mathbf{y}_k \geq |\boldsymbol{x}_k|^2, k = 1, \ldots, K\}$, the following inequality holds true for all $c > 0$:

$$\ln\left(1+\frac{1}{c}\sum_{k=1}^{K}\left(1-\frac{|\boldsymbol{x}_k|^2}{\mathbf{y}_k}\right)\right) \leq \quad (2a)$$

$$\ln\left(1+\frac{1}{c}\sum_{k=1}^{K}\left(1-\frac{|\bar{x}_k|^2}{\bar{y}_k}\right)\right) + \left(c+\sum_{k=1}^{K}\left(1-\frac{|\bar{x}_k|^2}{\bar{y}_k}\right)\right)^{-1}\sum_{k=1}^{K}\frac{|\bar{x}_k|^2}{\bar{y}_k} - \left(c+\sum_{k=1}^{K}\left(1-\frac{|\bar{x}_k|^2}{\bar{y}_k}\right)\right)^{-1} \times \sum_{k=1}^{K}\left(\frac{2\Re\left\{\bar{x}_k^H\boldsymbol{x}_k\right\}}{\bar{y}_k} - \frac{|\bar{x}_k|^2}{(\bar{y}_k)^2}\mathbf{y}_k\right). \quad (2b)$$

In fact, the function defined by (2b) is the linearization of that defined by (2a) at $(\bar{x}_k, \bar{y}_k), k = 1, \ldots, K$. Since the former is concave, it provides a tight majorant of the latter [34]. As such minimizing the former, called tight majorant minimization, helps to generate a better point than $(\bar{x}, \bar{y})$ for the latter.

II. Active-RIS aided OFDM System

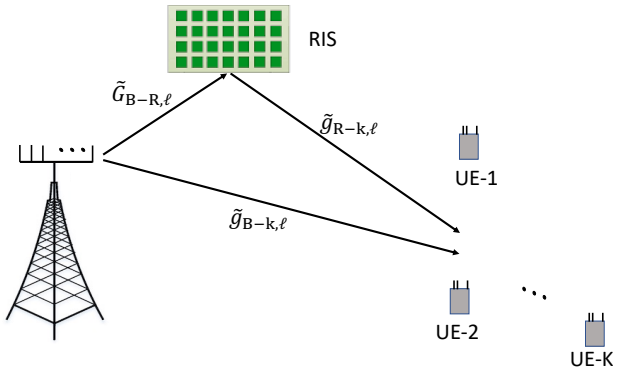

Fig. 1: Active RIS-assisted communication network

We consider the active-RIS-assisted MU MC system illustrated by Fig. 1, where an active-RIS of N reflecting units supports downlink transmission from an N_t-antenna array aided base station (BS) to K single-antenna users (UEs) $k \in \mathcal{K} \triangleq \{1, \ldots, K\}$. It is reasonable to assume the presence of a line-of-sight (LoS) link between the BS and RIS as well as between the RIS and UEs because the RIS is frequently installed on the facade of high-rise buildings and the BS is also normally at a particular elevated height [2].

We consider signal propagation subject to multi-path effects, resulting in frequency-selective channels. We denote the channel gain matrix of the ℓ-th multiple-input multiple-output (MIMO) path between the BS and the RIS by $\tilde{G}_{\mathrm{B\text{-}R},\ell} = \sqrt{\beta_{\mathrm{B\text{-}R}}}G_{\mathrm{B\text{-}R},\ell} \in \mathbb{C}^{N\times N_t}$. Similarly, $\tilde{g}_{\mathrm{R\text{-}k},\ell} = \sqrt{\beta_{\mathrm{R\text{-}k}}}g_{\mathrm{R\text{-}k},\ell} \in$

TABLE I: Comparing our innovative contributions to the relevant literature.

Contents \ Literature	**This work**	[19]–[22]	[31], [32]	[29]	[27]	[15]–[17]
MU MC	√		√	√	√	
Passive-RIS aided single-user MC		√				
Passive-RIS aided MU MC	√				√	
Active-RIS aided MU single-carrier	√					√
SR maximization	√		√	√	√	√
Active-RIS aided MU MC	√					
Individual rate enhancement	√					
Tractable large-scale computation	√					

TABLE II: Basic Notations

Notation	Description
$N_t/\mathcal{N}_t$	# of BS's transmit antennas / index set $\{1,\ldots,N_t\}$
$K/\mathcal{K}$	# of users / index set $\{1,\ldots,K\}$
$N/\mathcal{N}$	# of active-RIS PREs / index set $\{1,\ldots,N\}$
$S/\mathcal{S}$	# of subcarriers / index set $\{1,\ldots,S\}$
$L_1/L_2/L_3$	memory of the multipath BS-RIS / RIS-UE / BS-UE channel
L	$\max\{L_1+L_2-1, L_3\}$
$\boldsymbol{\upsilon} \triangleq (\boldsymbol{\upsilon}_1,\ldots,\boldsymbol{\upsilon}_N)^T$	design vector of active PREs
$\boldsymbol{\Upsilon} \triangleq \mathsf{diag}\,(\boldsymbol{\upsilon})$	design PREs' reflection coefficient matrix
$\mathbf{w}_k(s) \triangleq \left(\mathbf{w}_{k,1}(s),\ldots,\mathbf{w}_{k,N_t}(s)\right)^T$	user k' beamformer over subcarrier s
$\mathbf{w}(s) \triangleq (\mathbf{w}_1(s),\ldots,\mathbf{w}_{N_t}(s))^T$	cascaded vectors for all UEs' beamformers over subcarrier s
$\mathbf{w} \triangleq \{\mathbf{w}(s), s\in\mathcal{S}\}$	set of all beamformers
$w^{(\tau)}/\upsilon^{(\tau)}$	generated values of $\mathbf{w}/\boldsymbol{\Upsilon}$ at the $(\tau-1)$-st round
$r_{k,s}(\mathbf{w},\boldsymbol{\upsilon})$	achievable throughput of UE k over subcarrier s
$r_k(\mathbf{w},\boldsymbol{\upsilon})$	total achievable throughput of UE k
$P_{\text{BS}}/P_{\text{A}}$	maximum transmit power budget at the BS / the active RIS

$\mathbb{C}^{1\times N}$ represents the channel gain co-vector of the ℓ-th multiple-input single-output (MISO) path between the RIS and UE k, and $\tilde{g}_{\text{B-k},\ell} = \sqrt{\beta_{\text{B-k}}} g_{\text{B-k},\ell} \in \mathbb{C}^{1\times N_t}$ represents the channel co-vector of the ℓ-th MISO path between the BS and UE k, where $\beta_{\text{B-R}}$, $\beta_{\text{R-k}}$, and $\beta_{\text{B-k}}$ represent the path-loss and large-scale fading of the BS-to-RIS link, the RIS-to-UE k link, and the BS-to-UE k link. Furthermore, due to the presence of the LoS link between the BS and the RIS and that between the RIS and UE k, their first respective channel paths, $G_{\text{B-R},0} \in \mathbb{C}^{N\times N_t}$ and $h_{\text{R-k},0} \in \mathbb{C}^{1\times N}$ are modeled by Rician fading, while the remaining channel paths $G_{\text{B-R},\ell} \in \mathbb{C}^{N\times N_t}$, for $\ell \neq 0$, and $g_{\text{R-k},\ell} \in \mathbb{C}^{1\times N}$, for $\ell \neq 0$, are modeled by Rayleigh fading [19]. On the other hand, all channel propagation paths between the BS and UE k, $g_{\text{B-k},\ell} \in \mathbb{C}^{1\times N_t}$, for all ℓ, follow Rayleigh fading to model the non-LoS propagation paths between the BS and UE k [19].

The frequency selective channels from the BS to RIS, from the RIS to UE k, and from the BS to UE k are characterized by the following transfer co-vector functions:

$$\bar{G}_{\text{B-R}}(z) \triangleq \sum_{\ell=0}^{L_1-1} \tilde{G}_{\text{B-R},\ell} z^{-\ell},$$
$$\bar{g}_{\text{R-k}}(z) \triangleq \sum_{\ell=0}^{L_2-1} \tilde{g}_{\text{R-k},\ell} z^{-\ell},$$
$$\bar{g}_{\text{B-k}}(z) \triangleq \sum_{\ell=0}^{L_3-1} \tilde{g}_{\text{B-k},\ell} z^{-\ell},$$

where L_1, L_2, and L_3 respectively define the memory of the multipath BS-RIS channel, the multipath RIS-UE channel, and the multipath BS-UE channel. Similar to numerous prior studies on RIS-aided beamforming [16], [17], [25], [27], the assumption of perfect CSI at the BS is commonly stipulated in order to evaluate the limit on the performance of the RIS-aided multi-user network. Tailor-made channel estimation solutions developed for RIS-aided networks can be harnessed for acquiring the CSI [23], [35]–[37].

For $n \in \mathcal{N} = \{1,\ldots,N\}$, let $\boldsymbol{\upsilon}_n = a_n\theta_n$, be the reflection coefficient of the n-th PRE at the active-RIS with a_n and θ_n representing its amplification factor and phase. Accordingly, we have

$$\boldsymbol{\Upsilon} \triangleq \mathsf{diag}\,(\boldsymbol{\upsilon}), \tag{3}$$

with $\boldsymbol{\upsilon} = (\boldsymbol{\upsilon}_1,\ldots,\boldsymbol{\upsilon}_N)^T \in \mathbb{C}^N$ is referred to as the PREs' reflection coefficient matrix. It is noteworthy that under active-RIS, the amplification factor a_n can be higher than one due to the use of an integrated reflection-type amplifier [15].

The composite channel spanning from the BS to UE k will also be frequency-selective and characterized by the transfer co-vector function

$$\hbar_k(z) = \bar{g}_{\text{R-k}}(z)\boldsymbol{\Upsilon}\bar{G}_{\text{B-R}}(z) + \bar{g}_{\text{B-k}}(z) \in \mathbb{C}^{1\times N_t}. \tag{4}$$

Let us assume that the system has $S = 2^Z$ sub-carriers, for some positive integer Z. At the i-th transmit antenna with $i \in \mathcal{N}_t \triangleq \{1,\ldots,N_t\}$, each block of information

$$x_i \triangleq \begin{bmatrix} x_i(0) \\ \cdots \\ x_i(S-1) \end{bmatrix},$$

of length S is processed by an orthogonal frequency division multiplexing (OFDM) operator to form an OFDM block of

length $S+L$:

$$\tilde{x}_i \triangleq \begin{bmatrix} x_{i,T} \\ x_{i,H} \\ x_{i,T} \end{bmatrix} \in \mathbb{C}^{S+L}$$

with

$$\begin{bmatrix} x_{i,H} \\ x_{i,T} \end{bmatrix} = F_S^H x_i, x_{i,H} \in \mathbb{C}^{S-L}, x_{i,T} \in \mathbb{C}^L,$$

where the OFDM cyclic prefix (CP) length is set to $L \geq \max\{L_1+L_2-1, L_3\}$ to avoid inter-block interference (IBI). The block $\tilde{x}_i$ of length $S+L$ is transmitted from the i-th transmit antenna. By discarding the first L entries of the received block and then applying the FFT, we obtain the received signal at each subcarrier $s \in \mathcal{S} \triangleq \{0, \ldots, S-1\}$ for UE k as

$$y_k(s) = \hbar_{k,s}(\boldsymbol{\upsilon}) x(s) + \bar{g}_{\text{R-k,s}} \boldsymbol{\Upsilon} \tilde{n} + n_k(s), \tag{5}$$

where

$$x(s) \triangleq \begin{bmatrix} x_1(s) \\ \ldots \\ x_{N_t}(s) \end{bmatrix} \in \mathbb{C}^{N_t}, \tag{6}$$

and $n_k(s)$ is the background noise of power σ^2,

$$\begin{aligned} \hbar_{k,s}(\boldsymbol{\upsilon}) &= \hbar_k(e^{\jmath 2\pi s/S}) & (7) \\ &= \bar{g}_{\text{R-k,s}} \mathsf{diag}(\boldsymbol{\upsilon}) G_{\text{B-R,s}} + \bar{g}_{\text{B-k,s}} & (8) \end{aligned}$$

with

$$\begin{aligned} \bar{g}_{\text{B-k,s}} &\triangleq \bar{g}_{\text{B-k}}(e^{\jmath 2\pi s/S}), \\ G_{\text{B-R,s}} &\triangleq G_{\text{B-R}}(e^{\jmath 2\pi s/S}), \\ \bar{g}_{\text{R-k,s}} &\triangleq \bar{g}_{\text{R-k}}(e^{\jmath 2\pi s/S}), \end{aligned}$$

and $\tilde{n} = (\tilde{n}_1, \ldots, \tilde{n}_N)^T \in \mathbb{C}^{N \times 1}$ is related to the input noise and the inherent device noise of the active-RIS elements and it is modeled as $\tilde{n}_n \sim \mathcal{CN}(0, \sigma_{\tilde{n}}^2)$. Therefore, $\boldsymbol{\Upsilon}\tilde{n}$ in (5) is the noise introduced and amplified by the reflection-type amplifier [38].

In MU beamforming, each $x(s) \in \mathbb{C}^{N_t}$ in (6) is given by

$$x(s) = \sum_{k=1}^{K} \mathbf{w}_k(s) u_k(s), \tag{9}$$

i.e. the information $u_k(s) \in \mathcal{C}(0,1)$ intended for UE k is beamformed by

$$\mathbf{w}_k(s) \triangleq \begin{bmatrix} \mathbf{w}_{k,1}(s) \\ \ldots \\ \mathbf{w}_{k,N_t}(s) \end{bmatrix} \in \mathbb{C}^{N_t}, k \in \mathcal{K}. \tag{10}$$

Thus, the received signal in (5) becomes

$$y_k(s) = \hbar_{k,s}(\boldsymbol{\upsilon}) \sum_{j=1}^{K} \mathbf{w}_j(s) u_j(s) + \bar{g}_{\text{R-k,s}} \boldsymbol{\Upsilon} \tilde{n} + n_k(s). \tag{11}$$

The transmit power constraint for the BS is given by

$$\left(1 + \frac{L}{S}\right) \sum_{k=1}^{K} \sum_{s=0}^{S-1} \|\mathbf{w}_k(s)\|^2 \leq P_{\text{BS}}, \tag{12}$$

where P_{BS} is the maximum transmit power budget at the BS. For active-RIS, we have to include a power constraint for the power reflected from the active-RIS, which is given by [15]

$$\left(1 + \frac{L}{S}\right) \left(\sum_{k=1}^{K} \sum_{s=0}^{S-1} \|\boldsymbol{\Upsilon} G_{\text{B-R,s}} \mathbf{w}_k(s)\|^2 + \|\boldsymbol{\Upsilon}\|^2 \sigma_{\tilde{n}}^2 \right) \leq P_{\text{A}}, \tag{13}$$

where P_{A} is the maximum transmit power budget at the active-RIS and (13) ensures that the power of the amplified signal reflected by the active RIS is less than P_{A}. Let

$$\mathbf{w}(s) \triangleq \begin{bmatrix} \mathbf{w}_1(s) \\ \ldots \\ \mathbf{w}_K(s) \end{bmatrix} \in \mathbb{C}^{KN_t},$$

and $\mathbf{w} \triangleq \{\mathbf{w}(s), s \in \mathcal{S}\}$. Then, using (11), the throughput of UE k over subcarrier s , in nats/sec, for our active-RIS-assisted OFDM communication system is given by (14) at the top of the page. Thus, the average rate of UE k is defined by

$$r_k(\mathbf{w}, \boldsymbol{\upsilon}) \triangleq \frac{1}{S} \sum_{s=0}^{S-1} r_{k,s}(\mathbf{w}(s), \boldsymbol{\upsilon}). \tag{15}$$

At the current state of research, the optimization of MU MC systems is primarily focused on maximizing the SR, formulated as:

$$\max_{\mathbf{w}, \boldsymbol{\upsilon}} \sum_{k=1}^{K} r_k(\mathbf{w}, \boldsymbol{\upsilon}) \quad \text{s.t.} \quad (12), (13).$$

However, our previous paper [29] has demonstrated that this approach leads to zero rates for certain users across the entire frequency band, rendering it unsuitable for MU MC communications. A promising technique of enhancing all user rates is based on max-min rate optimization formulated by

$$\max_{\mathbf{w}, \boldsymbol{\upsilon}} \min_{k=1,\ldots,K} r_k(\mathbf{w}, \boldsymbol{\upsilon}) \quad \text{s.t.} \quad (12), (13), \tag{16}$$

which constitutes a large-scale nonconvex problem, with its own computational challenges arising from the non-smooth nature of the MR objective function $\min_{k=1,\ldots,K} \ r_k(\mathbf{w}, \boldsymbol{\upsilon})$. To overcome the computational challenges associated with max-min rate optimization, we propose a pair of surrogate problems of smooth optimization that offer a more computationally tractable solution and enhance rate fairness: GM-rate optimization and soft max-min rate optimization. The subsequent sections provide further details on these surrogate problems.

III. GM-Rate Optimization for Active-RIS Aided OFDM Systems

This section addresses the joint design of the beamformers' weight set $\mathbf{w}$ and the vector $\boldsymbol{\upsilon}$ of PREs to maximize the GM of the users' rates for our active-RIS-assisted OFDM communication system, which can be formulated as:

$$\max_{\mathbf{w}, \boldsymbol{\upsilon}} f(\mathbf{w}, \boldsymbol{\upsilon}) \triangleq \left(\prod_{k=1}^{K} r_k(\mathbf{w}, \boldsymbol{\upsilon}) \right)^{1/K} \quad \text{s.t.} \quad (12), (13). \tag{17}$$

Our previous treatises [10], [11] on single carrier systems have demonstrated the effectiveness of GM-rate optimization in

$$r_{k,s}(\mathbf{w}(s),\boldsymbol{\upsilon})=\ln\left(1+\frac{|\hbar_{k,s}(\boldsymbol{\upsilon})\mathbf{w}_k(s)|^2}{\sum_{j\in\mathcal{K}\setminus\{k\}}|\hbar_{k,s}(\boldsymbol{\upsilon})\mathbf{w}_j(s)|^2+\|\bar{g}_{\text{R-k,s}}\boldsymbol{\Upsilon}\|^2\sigma_{\tilde{n}}^2+\sigma^2}\right). \tag{14}$$

improving the MU rate fairness, while achieving competitive SR. Following these solutions, we represent (17) by the following max-min problem:

$$\max_{\mathbf{w},\boldsymbol{\upsilon}}\min_{\gamma_k>0,\prod_{k=1}^K\gamma_k\geq 1}\left[\sum_{k=1}^K\gamma_k r_k(\mathbf{w},\boldsymbol{\upsilon})\right]\quad\text{s.t.}\quad(12),(13). \tag{18}$$

Let $(w^{(\tau)},\upsilon^{(\tau)})$ be a feasible point for (18) that is found from the $(\tau-1)$-st round. Note that

$$\min_{\gamma_k>0,\prod_{k=1}^K\gamma_k\geq 1}\left[\sum_{k=1}^K\gamma_k r_k(w^{(\tau)},\upsilon^{(\tau)})\right] \tag{19}$$

is attained at

$$\gamma_k^{(\tau)}\triangleq\frac{\max\limits_{k'\in\mathcal{K}}r_{k'}(w^{(\tau)},\upsilon^{(\tau)})}{r_k(w^{(\tau)},\upsilon^{(\tau)})},\ k\in\mathcal{K}. \tag{20}$$

We solve the following problem at the τ-th iteration to generate $\left(w^{(\tau+1)},\upsilon^{(\tau+1)}\right)$:

$$\max_{\mathbf{w},\boldsymbol{\upsilon}}f^{(\tau)}(\mathbf{w},\boldsymbol{\upsilon})\triangleq\sum_{k=1}^K\gamma_k^{(\tau)}r_k(\mathbf{w},\boldsymbol{\upsilon})\quad\text{s.t.}\quad(12),(13). \tag{21}$$

A. Beamforming ascent

To seek $w^{(\tau+1)}$ so that the condition of

$$f^{(\tau)}(w^{(\tau+1)},\upsilon^{(\tau)})>f^{(\tau)}(w^{(\tau)},\upsilon^{(\tau)}), \tag{22}$$

is met, we consider the following optimization problem:

$$\max_{\mathbf{w}}\quad f^{(\tau)}(\mathbf{w},\upsilon^{(\tau)}) \tag{23a}$$

$$\text{s.t.}\quad\sum_{k=1}^K\sum_{s=0}^{S-1}\|\mathbf{w}_k(s)\|^2\leq\bar{P}_{\text{BS}}, \tag{23b}$$

$$\sum_{k=1}^K\sum_{s=0}^{S-1}\mathbf{w}_k^H(s)E_s\mathbf{w}_k(s)\ \leq\ \bar{P}_{\text{A}}, \tag{23c}$$

where

$$\begin{aligned}\bar{P}_{\text{BS}}&\triangleq\frac{P_{\text{BS}}}{1+\frac{L}{S}},\\ \bar{P}_{\text{A}}&\triangleq\frac{P_{\text{A}}}{1+\frac{L}{S}}-\|\Upsilon^{(\tau)}\|^2\sigma_{\tilde{n}}^2,\\ E_s&\triangleq\left(G_{\text{B-R,s}}\right)^H\left(\Upsilon^{(\tau)}\right)^H\Upsilon^{(\tau)}G_{\text{B-R,s}}.\end{aligned} \tag{24}$$

Using the inequality (1) for $\mathbf{v}=\hbar_{k,s}(\upsilon^{(\tau)})\mathbf{w}_k(s)$, $\mathbf{y}=\sum_{j\in\mathcal{K}\setminus\{k\}}|\hbar_{k,s}(\upsilon^{(\tau)})\mathbf{w}_j(s)|^2+\sigma_a^2$, and $\bar{v}=\hbar_{k,s}(\upsilon^{(\tau)})w_k^{(\tau)}(s)$, $\bar{y}=y_{k,s}^{(\tau)}\triangleq\sum_{j\in\mathcal{K}\setminus\{k\}}|\hbar_{k,s}(\upsilon^{(\tau)})w_j^{(\tau)}(s)|^2+\sigma_a^2$, for $\sigma_a^2=\|\bar{g}_{\text{R-k,s}}\Upsilon^{(\tau)}\|^2\sigma_{\tilde{n}}^2+\sigma^2$, yields the following tight concave minorant of $r_{k,s}(\mathbf{w}(s),\upsilon^{(\tau)})$ at $w^{(\tau)}(s)$:

$$\begin{aligned}r_{k,s}(\mathbf{w}(s),\upsilon^{(\tau)})&\geq r_{k,s}^{(\tau)}(\mathbf{w}(s))\\&\triangleq a_{k,s}^{(\tau)}+2\Re\{\langle b_{k,s}^{(\tau)},\mathbf{w}_k(s)\rangle\}\\&\quad-c_{k,s}^{(\tau)}\sum_{j=1}^K\left|\hbar_{k,s}(\upsilon^{(\tau)})\mathbf{w}_j(s)\right|^2,\end{aligned} \tag{25}$$

with

$$\begin{aligned}a_{k,s}^{(\tau)}&\triangleq r_{k,s}(\upsilon^{(\tau)},w^{(\tau)}(s))-\frac{|\hbar_{k,s}(\upsilon^{(\tau)})w_k^{(\tau)}(s)|^2}{y_{k,s}^{(\tau)}}-\sigma_a^2c_{k,s}^{(\tau)},\\ b_{k,s}^{(\tau)}&\triangleq\frac{\hbar_{k,s}(\upsilon^{(\tau)})w_k^{(\tau)}(s)}{y_{k,s}^{(\tau)}}(\hbar_{k,s}(\upsilon^{(\tau)}))^H,\\ 0<c_{k,s}^{(\tau)}&\triangleq\frac{|\hbar_{k,s}(\upsilon^{(\tau)})w_{k,s}^{(\tau)}|^2}{y_{k,s}^{(\tau)}\left(y_{k,s}^{(\tau)}+|\hbar_{k,s}(\upsilon^{(\tau)})w_k^{(\tau)}(s)|^2\right)}.\end{aligned} \tag{26}$$

Thus, using (25), a tight concave minorant of $f^{(\tau)}(\mathbf{w},\upsilon^{(\tau)})$ at $w^{(\tau)}$ is given by:

$$\begin{aligned}f_b^{(\tau)}(\mathbf{w})&\triangleq\sum_{k=1}^K\gamma_k^{(\tau)}\sum_{s=0}^{S-1}r_{k,s}^{(\tau)}(\mathbf{w}(s))\\&=\sum_{k=1}^K\gamma_k^{(\tau)}\sum_{s=0}^{S-1}a_{k,s}^{(\tau)}+2\sum_{k=1}^K\sum_{s=0}^{S-1}\Re\{\langle\bar{b}_{k,s}^{(\tau)},\mathbf{w}_k(s)\rangle\}\\&\quad-\sum_{s=0}^{S-1}\sum_{k=1}^K\mathbf{w}_k^H(s)\Psi_s^{(\tau)}\mathbf{w}_k(s),\end{aligned} \tag{27}$$

with

$$\begin{aligned}0\preceq\Psi_s^{(\tau)}&\triangleq\textstyle\sum_{j=1}^K\gamma_j^{(\tau)}c_{j,s}^{(\tau)}(\hbar_{j,s}(\upsilon^{(\tau)}))^H\hbar_{j,s}(\upsilon^{(\tau)}),\ s\in\mathcal{S},\\ \bar{b}_{k,s}^{(\tau)}&\triangleq\gamma_k^{(\tau)}b_{k,s}^{(\tau)}.\end{aligned} \tag{28}$$

Note that $f_b^{(\tau)}(\mathbf{w})$ in (27) is a tight concave minorant of $f^{(\tau)}(\mathbf{w},\upsilon^{(\tau)})$ because $r_{k,s}^{(\tau)}(\mathbf{w}(s))$ serves as a tight concave minorant of $r_{k,s}(\mathbf{w}(s),\upsilon^{(\tau)})$, as shown in (25).

Thus, a specific $w^{(\tau+1)}$ verifying (22) can be found as the optimal solution of the following convex problem of tight minorant maximization of (23)

$$\max_{\mathbf{w}}\quad f_b^{(\tau)}(\mathbf{w})\quad\text{s.t.}\quad(23\text{b}),(23\text{c}). \tag{29}$$

Since we have a pair of quadratic constraints in (29) due to the use of active-RIS, a simple bisection approach, as adopted in [28] in conjunction with a single quadratic constraint can no longer be applied. Hence a sophisticated bisection procedure based on iterating closed-form expressions is conceived for computing (29) in Appendix A, where the symbols $b_{k,s}$, $\boldsymbol{x}_{k,s}$, Q_s, P_1, P_2 are used in place of $\bar{b}_{k,s}^{(\tau)}$, $\mathbf{w}_k(s)$, $\Psi_s^{(\tau)}$, $\bar{P}_{\text{BS}}$, and $\bar{P}_{\text{A}}$.

B. PREs ascent

Upon using (5) , we have

$$\hbar_{k,s}(\boldsymbol{\upsilon})w_j^{(\tau+1)}(s)=q_{k,s,j}^{(\tau+1)}\boldsymbol{\upsilon}+\bar{g}_{\text{B-k,s}}w_j^{(\tau+1)}(s) \tag{30}$$

for

$$q_{k,s,j}^{(\tau+1)}=\left(w_j^{(\tau+1)}(s)\right)^T(G_{\text{B-R,s}})^TD_{k,s}\ \in\mathbb{C}^{1\times N},$$

$$r_{k,s}(w^{(\tau+1)}(s),\boldsymbol{\upsilon})=\ln\left(1+\frac{\left|q_{k,s,k}^{(\tau+1)}\boldsymbol{\upsilon}+\bar{g}_{\text{B-k,s}}w_k^{(\tau+1)}(s)\right|^2}{\sum_{j\in\mathcal{K}\setminus\{k\}}\left|q_{k,s,j}^{(\tau+1)}\boldsymbol{\upsilon}+\bar{g}_{\text{B-k,s}}w_j^{(\tau+1)}(s)\right|^2+\|\sigma_{\tilde{n}}^2D_{k,s}\boldsymbol{\upsilon}\|^2+\sigma^2}\right). \tag{32}$$

$$k\in\mathcal{K},j\in\mathcal{K},n\in\mathcal{N},$$

where

$$D_{k,s}\triangleq\mathsf{diag}\left(\bar{g}_{\text{R-k,s}}\right). \tag{31}$$

Upon using (30), the throughput of $u_k(s)$ for UE k in (14) can be written as (32), which is provded at the top of the page.

To seek a specific $\upsilon^{(\tau+1)}$ so that the condition of

$$f^{(\tau)}(w^{(\tau+1)},\upsilon^{(\tau+1)})>f^{(\tau)}(w^{(\tau+1)},\upsilon^{(\tau)}) \tag{33}$$

is met, we consider the following problem:

$$\max_{\boldsymbol{\upsilon}}\ f^{(\tau)}(w^{(\tau+1)},\boldsymbol{\upsilon}) \tag{34a}$$

$$\text{s.t.}\quad\left(1+\frac{L}{S}\right)\boldsymbol{\upsilon}^HX^{(\tau)}\boldsymbol{\upsilon}\leq\ P_{\text{A}}, \tag{34b}$$

where

$$f^{(\tau)}(w^{(\tau+1)},\boldsymbol{\upsilon})\triangleq\sum_{k=1}^{K}\gamma_k^{(\tau)}\left(\frac{1}{S}\sum_{s=0}^{S-1}r_{k,s}(w^{(\tau+1)}(s),\boldsymbol{\upsilon})\right)$$

is obtained by using (15) and (21), and $X^{(\tau)}$ is defined as

$$\begin{aligned}X^{(\tau)}\ &\triangleq\ \sum_{k=1}^{K}\sum_{s=0}^{S-1}\mathsf{diag}\left(G_{\text{B-R,s}}w_k^{(\tau+1)}(s)\right)^H\\&\quad\times\mathsf{diag}\left(G_{\text{B-R,s}}w_k^{(\tau+1)}(s)\right)+\sigma_{\tilde{n}}^2I_N.\end{aligned} \tag{35}$$

Using the inequality (1) for $\mathbf{v}=q_{k,s,k}^{(\tau+1)}\boldsymbol{\upsilon}+\bar{g}_{\text{B-k,s}}w_k^{(\tau+1)}(s)$, $\mathbf{y}=\sum_{j\in\mathcal{K}\setminus\{k\}}\left|q_{k,s,j}^{(\tau+1)}\boldsymbol{\upsilon}+\bar{g}_{\text{B-k,s}}w_j^{(\tau+1)}(s)\right|^2+\|\sigma_{\tilde{n}}^2D_{k,s}\boldsymbol{\upsilon}\|^2+\sigma^2$, and $\bar{v}=q_{k,s,k}^{(\tau+1)}\upsilon^{(\tau)}+\bar{g}_{\text{B-k,s}}w_k^{(\tau+1)}(s)$, $\bar{y}=y_{k,s}^{(\tau)}\triangleq\sum_{j\in\mathcal{K}\setminus\{k\}}\left|q_{k,s,j}^{(\tau+1)}\upsilon^{(\tau)}+\bar{g}_{\text{B-k,s}}w_j^{(\tau+1)}(s)\right|^2+\|\sigma_{\tilde{n}}^2D_{k,s}\upsilon^{(\tau)}\|^2+\sigma^2$, yields the following tight concave minorant of $r_{k,s}(w^{(\tau+1)}(s),\boldsymbol{\upsilon})$ at $\upsilon^{(\tau)}$:

$$\begin{aligned}r_{k,s}(w^{(\tau+1)}(s),\boldsymbol{\upsilon})&\geq r_{k,s}^{(\tau)}(\boldsymbol{\upsilon})\\&\triangleq a_{k,s}^{(\tau)}+2\Re\{b_{k,s}^{(\tau)}\boldsymbol{\upsilon}\}\\&\quad-c_{k,s}^{(\tau)}\left(\sum_{j=1}^{K}\left|q_{k,s,j}^{(\tau+1)}\boldsymbol{\upsilon}\right|^2+\left\|\sigma_{\tilde{n}}^2D_{k,s}\boldsymbol{\upsilon}\right\|^2\right),\\&=a_{k,s}^{(\tau)}+2\Re\left\{b_{k,s}^{(\tau)}\boldsymbol{\upsilon}\right\}-c_{k,s}^{(\tau)}\boldsymbol{\upsilon}^H\Phi_{k,s}^{(\tau)}\boldsymbol{\upsilon},\end{aligned} \tag{36}$$

with

$$\begin{aligned}a_{k,s}^{(\tau)}&\triangleq r_{k,s}(w^{(\tau+1)},\upsilon^{(\tau)})-\frac{|\rho_{k,s}^{(\tau)}|^2}{y_{k,s}^{(\tau+1)}}\\&\quad+2\Re\left\{\frac{\left(\rho_{k,s}^{(\tau)}\right)^*}{y_{k,s}^{(\tau+1)}}\left(\bar{g}_{\text{B-k,s}}w_k^{(\tau+1)}(s)\right)\right\}\\&\quad-c_{k,s}^{(\tau)}\left(\textstyle\sum_{j=1}^{K}\left|\bar{g}_{\text{B-k,s}}w_j^{(\tau+1)}(s)\right|^2+\sigma^2\right)\\b_{k,s}^{(\tau)}&\triangleq\frac{\left(\rho_{k,s}^{(\tau)}\right)^*}{y_{k,s}^{(\tau+1)}}q_{k,s,k}^{(\tau+1)}-c_{k,s}^{(\tau)}\sum_{j=1}^{K}\left(\bar{g}_{\text{B-k,s}}w_j^{(\tau+1)}(s)\right)^*q_{k,s,j}^{(\tau+1)}\\0<c_{k,s}^{(\tau)}&\triangleq\frac{|\rho_{k,s}^{(\tau)}|^2}{y_{k,s}^{(\tau+1)}\left(y_{k,s}^{(\tau+1)}+\left|\rho_{k,s}^{(\tau)}\right|^2\right)}\\\rho_{k,s}^{(\tau)}&\triangleq q_{k,s,k}^{(\tau+1)}\upsilon^{(\tau)}+\bar{g}_{\text{B-k,s}}w_k^{(\tau+1)}(s)\ \in\mathbb{C}\\\Phi_{k,s}^{(\tau)}&\triangleq\textstyle\sum_{j=1}^{K}\left(q_{k,s,j}^{(\tau+1)}\right)^Hq_{k,s,j}^{(\tau+1)}+\sigma_{\tilde{n}}^2D_{k,s}^HD_{k,s}\ \in\mathbb{C}^{N\times N}.\end{aligned}$$

Thus, upon using (36), a tight concave minorant of $f^{(\tau)}(w^{(\tau+1)},\boldsymbol{\upsilon})$ at $\upsilon^{(\tau)}$ is given by:

$$\begin{aligned}f_c^{(\tau)}(\boldsymbol{\upsilon})\ &\triangleq\ \sum_{k=1}^{K}\gamma_k^{(\tau)}\sum_{s=0}^{S-1}r_{k,s}^{(\tau)}(\boldsymbol{\upsilon})\\&=\ a^{(\tau)}+2\Re\{b^{(\tau)}\boldsymbol{\upsilon}\}-\boldsymbol{\upsilon}^H\Psi^{(\tau)}\boldsymbol{\upsilon},\end{aligned} \tag{37}$$

with $a^{(\tau)}\triangleq\sum_{k=1}^{K}\gamma_k^{(\tau)}\sum_{s=0}^{S-1}a_{k,s}^{(\tau)}$, $b^{(\tau)}\triangleq\sum_{k=1}^{K}\gamma_k^{(\tau)}\sum_{s=0}^{S-1}b_{k,s}^{(\tau)}$, and $0\preceq\Psi^{(\tau)}\triangleq\sum_{k=1}^{K}\gamma_k^{(\tau)}\sum_{s=0}^{S-1}c_{k,s}^{(\tau)}\Phi_{k,s}^{(\tau)}$.

Thus, a particular $\upsilon^{(\tau+1)}$ verifying (33) can be found as the optimal solution of the following convex problem of tight minorant maximization of (34)

$$\max_{\boldsymbol{\upsilon}}\ f_c^{(\tau)}(\boldsymbol{\upsilon})\quad\text{s.t.}\quad\text{(34b)}, \tag{38}$$

which admits the closed-form solution

$$\upsilon^{(\tau+1)}=\begin{cases}\left(\Psi^{(\tau)}\right)^{-1}\left(b^{(\tau)}\right)^H & \text{if}\quad\Xi\leq\ P_{\text{A}},\\\left(\Psi^{(\tau)}+\mu X^{(\tau)}\right)^{-1}\left(b^{(\tau)}\right)^H & \text{otherwise},\end{cases} \tag{39}$$

where $\Xi\triangleq\left(1+\frac{L}{S}\right)\left(\upsilon^{(\tau)}\right)^HX^{(\tau)}\upsilon^{(\tau)}$ and $\mu>0$ is chosen by bisection for ensuring that $\left(1+\frac{L}{S}\right)\left(\upsilon^{(\tau)}\right)^HX^{(\tau)}\upsilon^{(\tau)}=\ P_{\text{A}}$. The solution in (39) can be explained as follows. If $\Xi\leq\ P_{\text{A}}$, we have to solve for unconstrained optimization

$$\max_{\boldsymbol{\upsilon}}\ f_c^{(\tau)}(\boldsymbol{\upsilon})\triangleq a^{(\tau)}+2\Re\{b^{(\tau)}\boldsymbol{\upsilon}\}-\boldsymbol{\upsilon}^H\Psi^{(\tau)}\boldsymbol{\upsilon}.$$

Taking the derivative of $f_c^{(\tau)}(\boldsymbol{\upsilon})$ with respect to $\boldsymbol{\upsilon}$ and equating the result to zero yields the first expression in the case equation (39). On the other hand, if $\Xi>\ P_{\text{A}}$, we can introduce a Lagrangian parameter μ and solve the following optimization problem:

$$\max_{\boldsymbol{\upsilon}}\ f_c^{(\tau)}(\boldsymbol{\upsilon})-\mu\left(\left(1+\frac{L}{S}\right)\left(\upsilon^{(\tau)}\right)^HX^{(\tau)}\upsilon^{(\tau)}-\ P_{\text{A}}\right).$$

By taking the derivative of the above objective function with respect to $\boldsymbol{\upsilon}$ and equating the result to zero yields the second expression in the case equation (39).

Algorithm 1 provides the pseudo-code for the proposed steep descent procedure of computing (17). Although (22) and (33) only show that $f^{(\tau)}\left(w^{(\tau+1)},\upsilon^{(\tau+1)}\right) > f^{(\tau)}\left(w^{(\tau)},\upsilon^{(\tau)}\right)$, our simulations confirm that Algorithm 1 also achieves

$$f\left(w^{(\tau+1)},\upsilon^{(\tau+1)}\right) > f\left(w^{(\tau)},\upsilon^{(\tau)}\right), \tag{40}$$

i.e. there is no need for line search to find a better feasible point than the incumbent $(w^{(\tau)},\upsilon^{(\tau)})$. Therefore, the sequence $\{(w^{(\tau)},\upsilon^{(\tau)})\}$ of improved feasible points for the GM-rate problem (17) is seen to be convergent by Cauchy's theorem.

Algorithm 1 GM-rate optimization algorithm for active-RIS aided MU MC system

1: **Initialization:** Set $\tau = 0$. Generate random $(w^{(0)},\upsilon^{(0)})$ meeting the constraints (12) and (13). Caclulate $\gamma_k^{(0)}$ by (21).
2: **Repeat until convergence of the objective function in** (17)**:** Generate $w^{(\tau+1)}$ by solving (29) using the procedure proposed in Appendix A. Generate $\upsilon^{(\tau+1)}$ by (39). Reset $\tau = \tau + 1$.
3: **Output** $(w^{(\tau)},\theta^{(\tau)})$ and user rates $r_k(w^{(\tau)},\upsilon^{(\tau)})$, $k \in \mathcal{K}$.

IV. Soft Max-Min Rate Optimization for Active-RIS Aided OFDM Systems

In this section, we introduce another surrogate optimization problem, which we refer to as "soft max-min (SMM) rate optimization". This problem is formulated based on a soft and smooth approximation of the non-smooth MR function.

We have

$$r_k(\mathbf{w},\boldsymbol{\upsilon}) = -\frac{1}{S}\sum_{s\in\mathcal{S}}\ln\left(1+\frac{|\hbar_{k,s}(\boldsymbol{\upsilon})\mathbf{w}_k(s)|^2}{\phi_{k,s}(\mathbf{w},\boldsymbol{\upsilon})}\right)^{-1} \tag{41}$$

$$\geq -\ln\left[\frac{1}{S}\sum_{s\in\mathcal{S}}\left(1+\frac{|\hbar_{k,s}(\boldsymbol{\upsilon})\mathbf{w}_k(s)|^2}{\phi_{k,s}(\mathbf{w},\boldsymbol{\upsilon})}\right)^{-1}\right] \tag{42}$$

$$= \ln S + \ln\left[\sum_{s\in\mathcal{S}}\left(1+\frac{|\hbar_{k,s}(\boldsymbol{\upsilon})\mathbf{w}_k(s)|^2}{\phi_{k,s}(\mathbf{w},\boldsymbol{\upsilon})}\right)^{-1}\right]^{-1}. \tag{43}$$

for

$$\phi_{k,s}(\mathbf{w},\boldsymbol{\upsilon}) \triangleq \sum_{j\in\mathcal{K}\setminus\{k\}}|\hbar_{k,s}(\boldsymbol{\upsilon})\mathbf{w}_j(s)|^2 + \|\bar{g}_{\text{R-k,s}}\boldsymbol{\Upsilon}\|^2\sigma_{\tilde{n}}^2+\sigma^2$$

The steps of obtaining (42) from (41) are provided in Appendix B. Instead of (16), we consider its minorant maximization

$$\max_{\mathbf{w},\boldsymbol{\upsilon}}\min_{k\in\mathcal{K}}\left\{\ln\left[\sum_{s\in\mathcal{S}}\left(1+\frac{|\hbar_{k,s}(\boldsymbol{\upsilon})\mathbf{w}_k(s)|^2}{\phi_{k,s}(\mathbf{w},\boldsymbol{\upsilon})}\right)^{-1}\right]^{-1}\right\} \tag{44}$$

$$\Leftrightarrow \quad \max_{\mathbf{w},\boldsymbol{\upsilon}}\left\{\max_{k\in\mathcal{K}}\sum_{s\in\mathcal{S}}\left(1+\frac{|\hbar_{k,s}(\boldsymbol{\upsilon})\mathbf{w}_k(s)|^2}{\phi_{k,s}(\mathbf{w},\boldsymbol{\upsilon})}\right)^{-1}\right\}^{-1} \tag{45}$$

$$\Leftrightarrow \quad \min_{\mathbf{w},\boldsymbol{\upsilon}}\max_{k\in\mathcal{K}}\sum_{s\in\mathcal{S}}\left(1+\frac{|\hbar_{k,s}(\boldsymbol{\upsilon})\mathbf{w}_k(s)|^2}{\phi_{k,s}(\mathbf{w},\boldsymbol{\upsilon})}\right)^{-1} \tag{46}$$

$$\Leftrightarrow \quad \min_{\mathbf{w},\boldsymbol{\upsilon}}\max_{k\in\mathcal{K}}\ln\left[1+\frac{1}{c}\sum_{s\in\mathcal{S}}\left(1+\frac{|\hbar_{k,s}(\boldsymbol{\upsilon})\mathbf{w}_k(s)|^2}{\phi_{k,s}(\mathbf{w},\boldsymbol{\upsilon})}\right)^{-1}\right] \tag{47}$$

for $c > 0$, while

$$\max_{k\in\mathcal{K}}\ln\left[1+\frac{1}{c}\sum_{s\in\mathcal{S}}\left(1+\frac{|\hbar_{k,s}(\boldsymbol{\upsilon})\mathbf{w}_k(s)|^2}{\phi_{k,s}(\mathbf{w},\boldsymbol{\upsilon})}\right)^{-1}\right] \leq \tag{48}$$

$$\ln\left[\sum_{k\in\mathcal{K}}\left(1+\frac{1}{c}\sum_{s\in\mathcal{S}}\left(1+\frac{|\hbar_{k,s}(\boldsymbol{\upsilon})\mathbf{w}_k(s)|^2}{\phi_{k,s}(\mathbf{w},\boldsymbol{\upsilon})}\right)^{-1}\right)\right] = \tag{49}$$

$$\ln\left[\frac{1}{K}\sum_{k\in\mathcal{K}}\left(1+\frac{1}{c}\sum_{s\in\mathcal{S}}\left(1+\frac{|\hbar_{k,s}(\boldsymbol{\upsilon})\mathbf{w}_k(s)|^2}{\phi_{k,s}(\mathbf{w},\boldsymbol{\upsilon})}\right)^{-1}\right)\right] + \ln K \leq \tag{50}$$

$$\max_{k\in\mathcal{K}}\ln\left[1+\frac{1}{c}\sum_{s\in\mathcal{S}}\left(1+\frac{|\hbar_{k,s}(\boldsymbol{\upsilon})\mathbf{w}_k(s)|^2}{\phi_{k,s}(\mathbf{w},\boldsymbol{\upsilon})}\right)^{-1}\right] + \ln K. \tag{51}$$

For small $c > 0$, the constant $\ln K$ becomes very small compared to the LHS of (48), so the first term in the LHS of (50) is an accurate approximation for the LHS of (48). We now address the max-min rate optimization problem (16) via the following soft max-min rate optimization problem:

$$\min_{\mathbf{w},\boldsymbol{\upsilon}}\ \ln\left[\frac{1}{K}\sum_{k\in\mathcal{K}}\left(1+\frac{1}{c}\sum_{s\in\mathcal{S}}\left(1+\frac{|\hbar_{k,s}(\boldsymbol{\upsilon})\mathbf{w}_k(s)|^2}{\phi_{k,s}(\mathbf{w},\boldsymbol{\upsilon})}\right)^{-1}\right)\right]$$
$$\text{s.t.}\quad (12),(13), \tag{52}$$

which is rewritten as

$$\min_{\mathbf{w},\boldsymbol{\upsilon}}\ \tilde{f}(\mathbf{w},\boldsymbol{\upsilon}) \triangleq \ln\left[1+\frac{1}{c}\sum_{k\in\mathcal{K}}\sum_{s\in\mathcal{S}}\left(1-\frac{|\hbar_{k,s}(\boldsymbol{\upsilon})\mathbf{w}_k(s)|^2}{\bar{\phi}_{k,s}(\mathbf{w},\boldsymbol{\upsilon})}\right)\right]$$
$$\text{s.t.}\quad (12),(13). \tag{53}$$

for

$$\bar{\phi}_{k,s}(\mathbf{w},\boldsymbol{\upsilon}) \triangleq \phi_{k,s}(\mathbf{w},\boldsymbol{\upsilon}) + |\hbar_{k,s}(\boldsymbol{\upsilon})\mathbf{w}_k(s)|^2$$
$$= \sum_{j\in\mathcal{K}}|\hbar_{k,s}(\boldsymbol{\upsilon})\mathbf{w}_j(s)|^2 + \|\bar{g}_{\text{R-k,s}}\boldsymbol{\Upsilon}\|^2\sigma_{\tilde{n}}^2+\sigma^2$$

Let $(w^{(\tau)},\upsilon^{(\tau)})$ be the feasible point for (53) that is found from the $(\tau-1)$-th round.

A. Beamforming alternating optimization

To seek a particular $w^{(\tau+1)}$, so that the condition of

$$\tilde{f}(w^{(\tau+1)},\upsilon^{(\tau)}) > \tilde{f}(w^{(\tau)},\upsilon^{(\tau)}) \tag{54}$$

is met, we consider the following problem:

$$\min_{\mathbf{w}}\quad \tilde{f}(\mathbf{w},\upsilon^{(\tau)}) \triangleq \ln\left[1+\frac{1}{c}\sum_{k\in\mathcal{K}}\sum_{s\in\mathcal{S}}\left(1-\frac{\left|\hbar_{k,s}(\upsilon^{(\tau)})\mathbf{w}_k(s)\right|^2}{\sum_{j\in\mathcal{K}}\left|\hbar_{k,s}(\upsilon^{(\tau)})\mathbf{w}_j(s)\right|^2+\sigma_a^2}\right)\right]$$
$$\text{s.t.}\quad (23b),(23c), \tag{55}$$

where $\sigma_a^2 \triangleq \|\bar{g}_{\text{R-k,s}}\Upsilon^{(\tau)}\|^2\sigma_{\tilde{n}}^2+\sigma^2$. Using the inequality (2) for $\boldsymbol{x} = \hbar_{k,s}(\upsilon^{(\tau)})\mathbf{w}_k(s)$, $\mathbf{y} = \sum_{j\in\mathcal{K}}|\hbar_{k,s}(\upsilon^{(\tau)})\mathbf{w}_j(s)|^2+\sigma_a^2$, and $\bar{x} = \hbar_{k,s}(\upsilon^{(\tau)})w_k^{(\tau)}(s)$, $\bar{y} = y_{k,s}^{(\tau)} \triangleq \sum_{j\in\mathcal{K}}|\hbar_{k,s}(\upsilon^{(\tau)})w_j^{(\tau)}(s)|^2+\sigma_a^2$, yields the following tight majorant of $\tilde{f}(\mathbf{w},\upsilon^{(\tau)})$ at $w^{(\tau)}$:

$$\begin{aligned}\tilde{f}_b^{(\tau)}(\mathbf{w}) &\triangleq a^{(\tau)} - \sum_{k=1}^{K}\sum_{s=0}^{S-1}\Bigg(2\Re\{\langle b_{k,s}^{(\tau)},\mathbf{w}_k(s)\rangle\} \\ &\quad -c_{k,s}^{(\tau)}\sum_{j=1}^{K}|\hbar_{k,s}(\upsilon^{(\tau)})\mathbf{w}_j(s)|^2\Bigg), \\ &= a^{(\tau)} - 2\sum_{k=1}^{K}\sum_{s=0}^{S-1}\Re\{\langle b_{k,s}^{(\tau)},\mathbf{w}_k(s)\rangle\} \\ &\quad +\sum_{s=0}^{S-1}\sum_{k=1}^{K}\mathbf{w}_k^H(s)\Psi_s^{(\tau)}\mathbf{w}_k(s) \end{aligned} \tag{56}$$

with

$$\begin{aligned}&a^{(\tau)} \triangleq \ln\left(1+\frac{1}{c}\chi^{(\tau)}\right) \\ &\qquad +\sum_{k=1}^{K}\sum_{s=0}^{S-1}\left(\frac{|\hbar_{k,s}(\upsilon^{(\tau)})w_k^{(\tau)}(s)|^2}{y_{k,s}^{(\tau)}(c+\chi^{(\tau)})}+\sigma_a^2c_{k,s}^{(\tau)}\right), \\ &\chi^{(\tau)} \triangleq \sum_{k\in\mathcal{K}}\sum_{s\in\mathcal{S}}\left(1-\frac{|\hbar_{k,s}(\upsilon^{(\tau)})w_k^{(\tau)}(s)|^2}{\sum_{j\in\mathcal{K}}|\hbar_{k,s}(\upsilon^{(\tau)})w_j^{(\tau)}(s)|^2+\sigma_a^2}\right), \\ &b_{k,s}^{(\tau)} \triangleq \frac{\hbar_{k,s}(\upsilon^{(\tau)})w_k^{(\tau)}(s)}{y_{k,s}^{(\tau)}(c+\chi^{(\tau)})}\left(\hbar_{k,s}\right)^H, \\ &0<c_{k,s}^{(\tau)} \triangleq \frac{|\hbar_{k,s}(\upsilon^{(\tau)})w_{k,s}^{(\tau)}|^2}{\left(y_{k,s}^{(\tau)}\right)^2\left(c+\chi^{(\tau)}\right)}, \\ &0 \preceq \Psi_s^{(\tau)} \triangleq \sum_{j=1}^{K}c_{j,s}^{(\tau)}\left(\hbar_{j,s}(\upsilon^{(\tau)})\right)^H\hbar_{j,s}(\upsilon^{(\tau)}),\ s\in\mathcal{S}. \end{aligned} \tag{57}$$

We thus solve the following convex problem of majorant minimization for (55) to generate $w^{(\tau+1)}$, verifying (54):

$$\min_{\mathbf{w}}\ \tilde{f}_b^{(\tau)}(\mathbf{w}) \quad \text{s.t.} \quad (23b),(23c). \tag{58}$$

An innovative bisection procedure, which is based on iterating closed-form expressions, for computing (58) is provided in Appendix A, where the symbols $b_{k,s}$, $\boldsymbol{x}_{k,s}$, Q_s, P_1, P_2 are used in place of $b_{k,s}^{(\tau)}$, $\mathbf{w}_k(s)$, $\Psi_s^{(\tau)}$, $\bar{P}_{\text{BS}}$, and $\bar{P}_{\text{A}}$.

B. PREs alternating optimization

To seek a specific $\upsilon^{(\tau+1)}$ so that

$$\tilde{f}(w^{(\tau+1)},\upsilon^{(\tau+1)}) > \tilde{f}(w^{(\tau+1)},\upsilon^{(\tau)}), \tag{59}$$

is met, we consider the following problem:

$$\min_{\boldsymbol{\upsilon}}\ \ln\left[1+\frac{1}{c}\sum_{k\in\mathcal{K}}\sum_{s\in\mathcal{S}}\left(1-\frac{\left|\hbar_{k,s}(\boldsymbol{\upsilon})w_k^{(\tau)}(s)\right|^2}{\sum_{j\in\mathcal{K}}\left|\hbar_{k,s}(\boldsymbol{\upsilon})w_j^{(\tau)}(s)\right|^2+\|\bar{g}_{\text{R-k,s}}\boldsymbol{\Upsilon}\|^2\sigma_{\tilde{n}}^2+\sigma^2}\right)\right] \tag{60a}$$

$$\text{s.t.}\quad \sum_{k=1}^{K}\sum_{s=0}^{S-1}\left\|\boldsymbol{\Upsilon}G_{\text{B-R,s}}w_k^{(\tau)}(s)\right\|^2+\|\boldsymbol{\Upsilon}\|^2\sigma_{\tilde{n}}^2 \le \widetilde{P}_{\text{A}}, \tag{60b}$$

where $\widetilde{P}_{\text{A}} \triangleq \frac{P_{\text{A}}}{1+\frac{L}{S}}$. By relying on (30), the problem (60b) can be expressed as:

$$\min_{\boldsymbol{\upsilon}}\quad \tilde{f}(w^{(\tau+1)},\boldsymbol{\upsilon}) \tag{61a}$$

$$\text{s.t.}\quad \boldsymbol{\upsilon}^HX^{(\tau)}\boldsymbol{\upsilon} \le \widetilde{P}_{\text{A}}, \tag{61b}$$

where

$$\tilde{f}(w^{(\tau+1)},\boldsymbol{\upsilon}) \triangleq \ln\left[1+\frac{1}{c}\sum_{k\in\mathcal{K}}\sum_{s\in\mathcal{S}}\left(1-\frac{\left|q_{k,s,k}^{(\tau+1)}\boldsymbol{\upsilon}+\bar{g}_{\text{B-k,s}}w_k^{(\tau+1)}(s)\right|^2}{\sum_{j\in\mathcal{K}}\left|q_{k,s,j}^{(\tau+1)}\boldsymbol{\upsilon}+\bar{g}_{\text{B-k,s}}w_j^{(\tau+1)}(s)\right|^2+\|\sigma_{\tilde{n}}^2D_{k,s}\boldsymbol{\upsilon}\|^2+\sigma^2}\right)\right], \tag{62}$$

with $D_{k,s}$ defined in (31), and $X^{(\tau)}$ defined in (35). Using the inequality (2) for $\boldsymbol{x} = q_{k,s,k}^{(\tau+1)}\boldsymbol{\upsilon}+\bar{g}_{\text{B-k,s}}w_k^{(\tau+1)}(s)$, $\mathbf{y} = \sum_{j\in\mathcal{K}}\left|q_{k,s,j}^{(\tau+1)}\boldsymbol{\upsilon}+\bar{g}_{\text{B-k,s}}w_j^{(\tau+1)}(s)\right|^2+\|\sigma_{\tilde{n}}^2D_{k,s}\boldsymbol{\upsilon}\|^2+\sigma^2$, and $\bar{x} = q_{k,s,k}^{(\tau+1)}\upsilon^{(\tau)}+\bar{g}_{\text{B-k,s}}w_k^{(\tau+1)}(s)$, $\bar{y} = y_{k,s}^{(\tau)} \triangleq \sum_{j\in\mathcal{K}}\left|q_{k,s,j}^{(\tau+1)}\upsilon^{(\tau)}+\bar{g}_{\text{B-k,s}}w_j^{(\tau+1)}(s)\right|^2+\|\sigma_{\tilde{n}}^2D_{k,s}\upsilon^{(\tau)}\|^2+\sigma^2$, yields the following tight majorant of $\tilde{f}(w^{(\tau+1)},\boldsymbol{\upsilon})$ at $\upsilon^{(\tau)}$:

$$\begin{aligned}\tilde{f}_c^{(\tau)}(\boldsymbol{\upsilon}) &\triangleq \tilde{a}^{(\tau)} - \sum_{k=1}^{K}\sum_{s=0}^{S-1}\Bigg(2\Re\{\tilde{b}_{k,s}^{(\tau)}\boldsymbol{\upsilon}\}-\tilde{c}_{k,s}^{(\tau)} \\ &\qquad \times\left(\sum_{j=1}^{K}\left|q_{k,s,j}^{(\tau+1)}\boldsymbol{\upsilon}\right|^2+\left\|\sigma_{\tilde{n}}^2D_{k,s}\boldsymbol{\upsilon}\right\|^2\right)\Bigg) \\ &= \tilde{a}^{(\tau)} - \sum_{k=1}^{K}\sum_{s=0}^{S-1}\left(2\Re\{\tilde{b}_{k,s}^{(\tau)}\boldsymbol{\upsilon}\}-\tilde{c}_{k,s}^{(\tau)}\boldsymbol{\upsilon}^H\Phi_{k,s}^{(\tau)}\boldsymbol{\upsilon}\right) \\ &= \tilde{a}^{(\tau)} - 2\Re\{\tilde{b}^{(\tau)}\boldsymbol{\upsilon}\}+\boldsymbol{\upsilon}^H\tilde{\Psi}^{(\tau)}\boldsymbol{\upsilon} \end{aligned} \tag{63}$$

with

$$\begin{aligned}\tilde{a}^{(\tau)} &\triangleq \ln\left(1+\frac{1}{c}\tilde{\chi}^{(\tau)}\right)+\sum_{k=1}^{K}\sum_{s=0}^{S-1}\Bigg(\frac{|\rho_{k,s}^{(\tau)}|^2}{\eta_{k,s}^{(\tau)}} \\ &\quad -2\Re\left\{\frac{\left(\rho_{k,s}^{(\tau)}\right)^*}{\eta_{k,s}^{(\tau)}}\left(\bar{g}_{\text{B-k,s}}w_k^{(\tau+1)}(s)\right)\right\} \\ &\quad +c_{k,s}^{(\tau)}\left(\sum_{j=1}^{K}\left|\bar{g}_{\text{B-k,s}}w_j^{(\tau+1)}(s)\right|^2+\sigma^2\right)\Bigg) \end{aligned}$$

$$\begin{aligned}&\eta_{k,s}^{(\tau)} \triangleq \tilde{y}_{k,s}^{(\tau)}(c+\tilde{\chi}^{(\tau)}), \\ &\tilde{\chi}^{(\tau)} \triangleq \sum_{k\in\mathcal{K}}\sum_{s\in\mathcal{S}}\left(1-\frac{\left|q_{k,s,k}^{(\tau+1)}\upsilon^{(\tau)}+\bar{g}_{\text{B-k,s}}w_k^{(\tau+1)}(s)\right|^2}{\varphi_{k,s}^{(\tau)}}\right), \\ &\varphi_{k,s}^{(\tau)} \triangleq \sum_{j\in\mathcal{K}}\left|q_{k,s,j}^{(\tau+1)}\upsilon^{(\tau)}+\bar{g}_{\text{B-k,s}}w_j^{(\tau+1)}(s)\right|^2 \\ &\qquad +\|\sigma_{\tilde{n}}^2D_{k,s}\upsilon^{(\tau)}\|^2+\sigma^2 \end{aligned}$$

$$\tilde{b}_{k,s}^{(\tau)} \triangleq \frac{\left(\rho_{k,s}^{(\tau)}\right)^*}{\eta_{k,s}^{(\tau)}} q_{k,s,k}^{(\tau+1)} - c_{k,s}^{(\tau)} \sum_{j=1}^{K} \left(\bar{g}_{\text{B-k,s}} w_j^{(\tau+1)}(s)\right)^* q_{k,s,j}^{(\tau+1)}$$

$$0 < \tilde{c}_{k,s}^{(\tau)} \triangleq \frac{|\rho_{k,s}^{(\tau)}|^2}{\left(\tilde{y}_{k,s}^{(\tau)}\right)^2 \left(c + \tilde{\chi}^{(\tau)}\right)}$$

$$\rho_{k,s}^{(\tau)} \triangleq q_{k,s,k}^{(\tau+1)} \upsilon^{(\tau)} + \bar{g}_{\text{B-k,s}} w_k^{(\tau+1)}(s) \ \in \mathbb{C}$$

$$\Phi_{k,s}^{(\tau)} \triangleq \sum_{j=1}^{K} \left(q_{k,s,j}^{(\tau+1)}\right)^H q_{k,s,j}^{(\tau+1)} + \sigma_{\tilde{n}}^2 D_{k,s}^H D_{k,s} \ \in \mathbb{C}^{N\times N}$$

$$\tilde{b}^{(\tau)} \triangleq \sum_{k=1}^{K} \sum_{s=0}^{S-1} \tilde{b}_{k,s}^{(\tau)}$$

$$0 \preceq \tilde{\Psi}^{(\tau)} \triangleq \sum_{k=1}^{K} \sum_{s=0}^{S-1} c_{k,s}^{(\tau)} \Phi_{k,s}^{(\tau)}.$$

We thus solve the following convex problem of majorant minimization for (60) to generate $\upsilon^{(\tau+1)}$, verifying (59):

$$\min_{\boldsymbol{\upsilon}} \quad \tilde{f}_c^{(\tau)}(\boldsymbol{\upsilon}) \quad \text{s.t.} \quad (61b), \tag{64}$$

which admits the closed-form solution:

$$\upsilon^{(\tau+1)} = \begin{cases} (\tilde{\Psi}^{(\tau)})^{-1} \left(\tilde{b}^{(\tau)}\right)^H & \text{if} \quad \bar{\Xi} \leq \ \widetilde{P}_{\text{A}}, \\ \left(\tilde{\Psi}^{(\tau)} + \mu X^{(\tau)}\right)^{-1} \left(\tilde{b}^{(\tau)}\right)^H & \text{otherwise}, \end{cases} \tag{65}$$

where $\bar{\Xi} \triangleq \left(\upsilon^{(\tau)}\right)^H X^{(\tau)} \upsilon^{(\tau)}$ and $\mu > 0$ is chosen by bisection, so that $\left(\upsilon^{(\tau)}\right)^H X^{(\tau)} \upsilon^{(\tau)} = \widetilde{P}_{\text{A}}$.

The pseudo-code for solving the problem (53) is provided in Algorithm 2. It follows from (54) and (59) that

$$\tilde{f}(w^{(\tau+1)}, \upsilon^{(\tau+1)}) < \tilde{f}(w^{(\tau)}, \upsilon^{(\tau)}), \tag{66}$$

so the sequence $\left\{\left(w^{(\tau)}, \upsilon^{(\tau)}\right)\right\}$ of improved feasible points for (53) converges to $(\bar{w}, \bar{v})$ by Cauchy's theorem.

Algorithm 2 Soft max-min rate optimization algorithm for active-RIS aided OFDM system

1: **Initialization:** Set $\tau = 0$. Generate $(w^{(0)}, \upsilon^{(0)})$ meeting the constraints (12) and (13).
2: **Repeat until convergence of the objective function in** (53)**:** Generate $w^{(\tau+1)}$ by solving (58) using the procedure proposed in Appendix VI. Generate $\upsilon^{(\tau+1)}$ by (65). Reset $\tau = \tau + 1$.
3: **Output** $(w^{(\tau)}, \upsilon^{(\tau)})$ and user rates $r_k(w^{(\tau)}, \upsilon^{(\tau)})$, $k \in \mathcal{K}$.

V. Numerical Results

In this section, we evaluate the performance of our algorithms. Unless otherwise specified, we assume $N_t = 10$ transmit-antennas at the BS and $N = 100$ PREs at the active-RIS. We define P as the total transmit power budget, so that $P := P_{\text{BS}} + P_{\text{A}} + N(P_{\text{DC}} + P_{\text{SW}})$, where $P_{\text{DC}} = -5$ dBm is the direct current biasing power consumed by the amplifiers of PREs and $P_{\text{SW}} = -10$ dBm is the power used by the phase-shift switch and control circuit in each PRE [39]. We set $P_{\text{BS}} = 0.99C$ and $P_{\text{A}} = 0.01C$, for $C \triangleq P_{\text{BS}} + P_{\text{A}}$. Unless stated otherwise, we set $P = 32$ dBm. The noise power spectral density is -174 dBm/Hz and the transmission bandwidth is $B = 10$ MHz. This implies that the noise power over the total bandwidth is -104 dBm. Thus, the noise power at the RIS receiver is $\sigma_{\tilde{n}}^2 = -104$ dBm and at the user-receiver over the subcarrier bandwidth is $\sigma^2 = -104 - 10\log_{10}(S)$ dBm. We set $S = 64$ subcarriers for our MC system. The convergence tolerance of the proposed algorithms is set to 10^{-3} and the channel parameters are described in the following paragraph.

We set the path-loss of the BS-to-UE k link at a distance $d_{B,k}$ to $\beta_{B,k} \triangleq \mathcal{G}_{\text{BS}} - 33.05 - 36.7\log_{10}(d_{B,k})$ (dB), that of the BS-to-RIS link at a distance $d_{B,R}$ to $\beta_{B,R} = \mathcal{G}_{\text{RIS}} + \mathcal{G}_{\text{BS}} - 35.9 - 22\log_{10}(d_{B,R})$ (dB), and that of the RIS-to-UE k link at a distance $d_{R,k}$ to $\beta_{R,k} \triangleq \mathcal{G}_{\text{RIS}} - 33.05 - 30\log_{10}(d_{R,k})$ (dB), where $\mathcal{G}_{\text{RIS}} = 5$ dBi and $\mathcal{G}_{\text{BS}} = 5$ dBi are the antenna gains of the BS and RIS elements [7], [40], [41]. The BS and the RIS are deployed at the coordinates of (40, 0, 25) meters and (0, 60, 40) meters in the three-dimensional (3D) space, respectively, while $K = 10$ UEs are randomly distributed in a (120×120)meter area right of the BS and the RIS. We consider an $L_3 = 12$-tap multipath channel between the BS and the UEs, $L_1 = 2$-tap multipath channel between the BS and the RIS, and $L_2 = 4$-tap multipath channel between the RIS and the UEs. As explained in Section II, the elements of normalized small-scale fading channel vector $h_{\text{B,k},\ell}$, for all ℓ, those of the channel matrix $G_{\text{B,R},\ell}$, for $\ell \neq 0$, and those of the channel vector $h_{\text{R,k},\ell}$, for $\ell \neq 0$, follow Rayleigh distribution. On the other hand, the elements of the first tap of the channel matrix, $G_{\text{B,R},0}$, and those of the first tap of the channel vector, $h_{\text{R,k},0}$, obey Rician distribution with Rician K-factors of 5 and 0 dB, respectively [19]. We assume a negative-exponentially decaying delay profile with the root-mean-square delay spread of T_s, for the symbol time $T_s = 1/B$.

For performance comparison and validation purposes, we compare the performance of the proposed active-RIS-based implementation to that of the RIS-less and passive-RIS-based implementations. Explicitly, the RIS-less implementation simply assumes having no RIS, relying solely on direct communication between the BS and the UEs. On the other hand, the passive-RIS implementation utilizes a conventional RIS having passive elements and does not have the active-RIS power constraint of (13), resulting in $P_{\text{BS}} + NP_{\text{SW}} \equiv P$.

Fig. 2 illustrates the convergence of Algorithm 1 for GM-rate optimization. It can be observed that the GM-rate objective monotonically increases, validating (40), and the algorithm achieves rapid convergence within $25-35$ iterations. Fig. 3 plots the rate distribution over 64 subcarriers by the proposed GM-rate and SMM-rate optimization Algorithms 1 and 2, at $P = 30$ dBm. We can observe that the achievable rate is well-balanced over all the subcarriers. Particularly, the SMM-rate optimization Algorithm 2 is more profound in rate balancing feature compared to the GM-rate optimization Algorithm 1.

Figs. 4 and 5 depict the achievable rates of individual UEs obtained using the proposed GM-rate and SMM-rate optimization Algorithms 1 and 2, at $P = 20$ dBm and $P = 30$ dBm, respectively. The results are compared to those obtained using SR maximization, which is carried out by adapting Algorithm 1 for $\gamma_k \equiv 1$ for all $k \in \mathcal{K}$. The SR maximization leads to zero rates for certain UEs, whereas the proposed GM-rate and SMM-rate optimization algorithms aim for balancing the rates of all UEs and avoid zero rates.

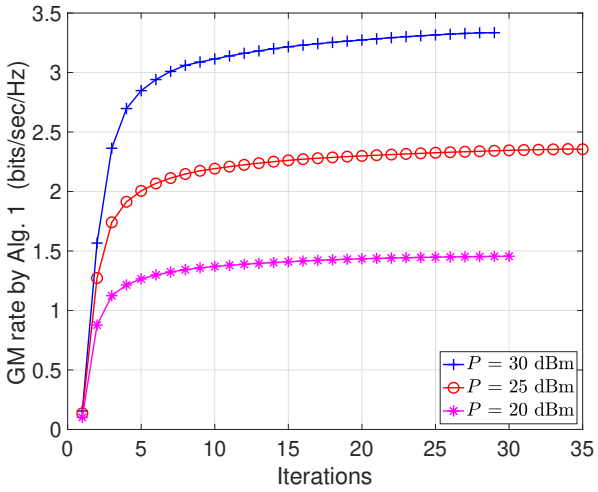

Fig. 2: Convergence of GM-rate optimization Alg. 1

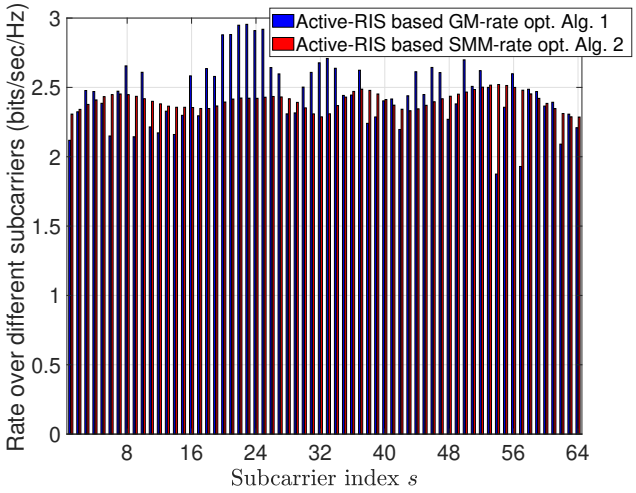

Fig. 3: Rate distribution over subcarriers at $P = 30$ dBm.

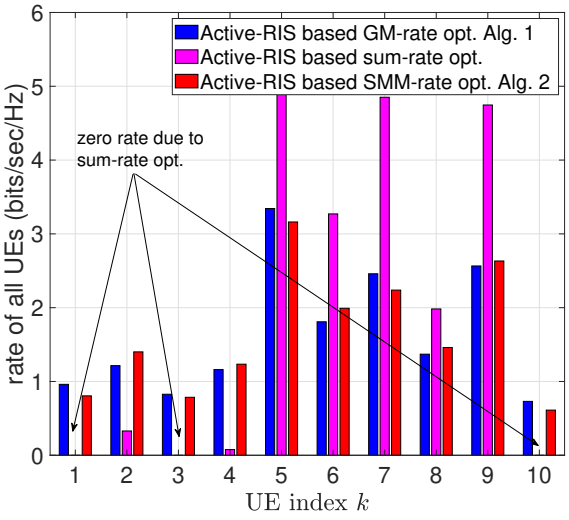

Fig. 4: Individual user-rates, $r_k(\mathbf{w}, \boldsymbol{\upsilon})$, for all users $k \in \mathcal{K}$ by different algorithms at $P = 20$ dBm.

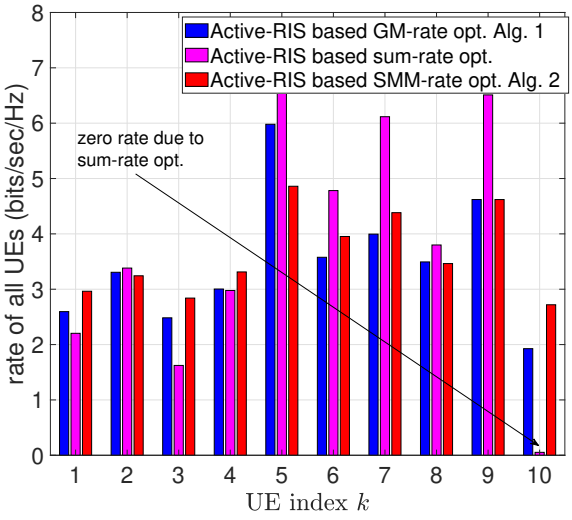

Fig. 5: Individual user-rates, $r_k(\mathbf{w}, \boldsymbol{\upsilon})$, for all users $k \in \mathcal{K}$ by different algorithms at $P = 30$ dBm.

In Fig. 6, the achievable MR is plotted against the total transmit power budget P. We can observe from Fig. 6 that the conventional passive-RIS-based implementation provides a modest performance advantage over the RIS-less-based implementation. On the other hand, Fig. 6 shows that the proposed active-RIS-based optimization algorithms outperform the conventional RIS-less or passive-RIS-based optimization methods. For example, considering SMM-rate optimization, the achievable MR of the active-RIS-based Algorithm 2 is 1.9 and 2.1 times higher than that of the passive-RIS and RIS-less based implementations, respectively, at $P = 32$ dBm. Similarly, upon considering GM-rate optimization, the achievable MR of the active-RIS Algorithm 1 is 1.8 times higher that of the respective passive-RIS and RIS-less based implementations at $P = 32$ dBm. This is because, in contrast to passive-RIS implementation, the use of active-RIS facilitates the power amplification of the incident signals. For a fair comparison, we ensure that both implementations are simulated under the same power budget. The details of this are provided at the start of Section V. Note that since we initialize the SMM-rate optimization Algorithm 2 by the solution of the GM-rate maximization Algorithm 1, the former outperforms the latter and the performance gap increases with the increase in P.

Fig. 6 demonstrates that the conventional passive-RIS-based implementation provides only a marginal performance advantage over the RIS-less implementation. By contrast, the proposed active-RIS-based optimization algorithms outperform both the passive-RIS and RIS-less methods. For instance, considering SMM-rate optimization, the achievable MR of the active-RIS Algorithm 2 is 1.9 and 2.1 times higher than that of the passive-RIS and RIS-less implementations, respectively, at $P = 32$ dBm. Similarly, for GM-rate optimization, the achievable MR of the active-RIS Algorithm 1 is 1.8 times higher than that of the respective passive-RIS and RIS-less

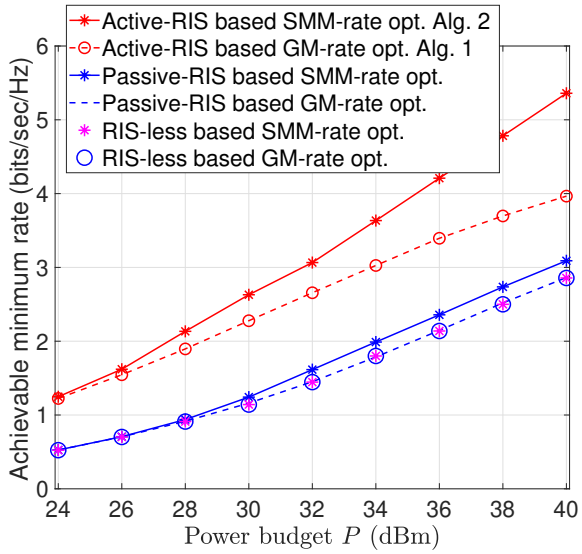

Fig. 6: Achievable MR versus the total transmit power budget P.

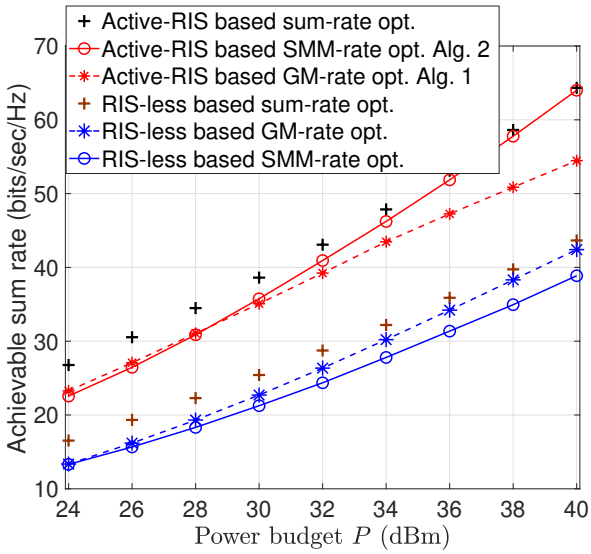

Fig. 7: Achievable SR versus the total transmit power budget P.

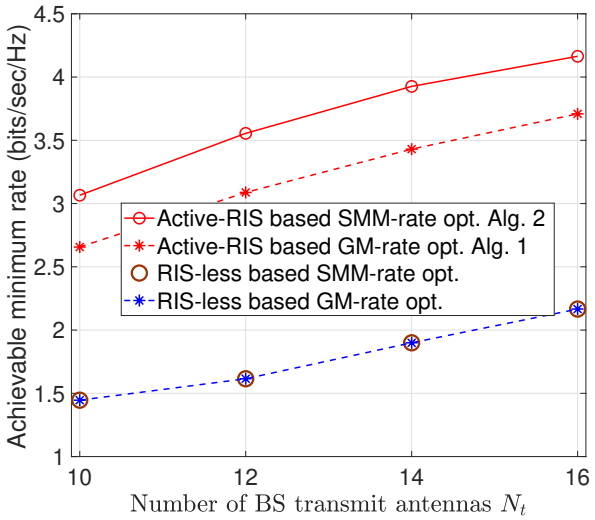

Fig. 8: Achievable MR versus the number of transmit antennas N_t.

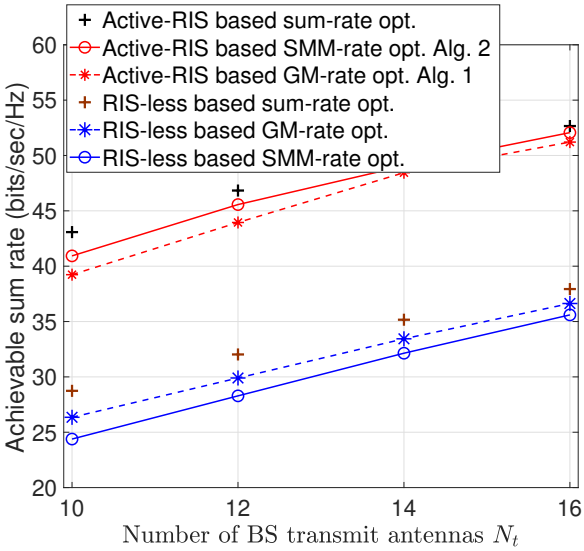

Fig. 9: Achievable SR versus the number of transmit antennas N_t.

implementations at $P = 32$ dBm. Moreover, since the SMM-rate optimization Algorithm 2 is initialized from the solution of the GM-rate maximization Algorithm 1, the former outperforms the latter in terms of its achievable MR, with the performance gap increasing upon increasing P.

Fig. 7 displays the achievable SR versus the total transmit power budget P. The proposed active-RIS-based optimization algorithms surpass the conventional RIS-less methods in terms of achievable SR. Additionally, the achievable SR using the SMM-rate optimization Algorithm 2 approaches that of SR maximization at higher power budgets. It is worth noting that SMM-rate optimization offers the advantage of fairer rate distribution among users and avoids zero rates for certain UEs, as already shown in Figs. 4 and 5.

Fig. 8 illustrates the achievable MR versus the number of transmit antennas N_t. The achievable MR increases upon increasing N_t due to the enhanced transmit antenna diversity. The superiority of the proposed active-RIS-based optimization algorithms over the conventional RIS-less methods is evident for various values of N_t. Notably, when initialized with the solution of the active-RIS-based GM-rate Algorithm 1, the SMM-rate optimization Algorithm 2 further enhances the MR by approximately 15% compared to the former across different N_t values.

Fig. 9 presents the achievable SR versus the number of transmit antennas N_t. Notably, the achievable SR using the SMM-rate optimization Algorithm 2 approaches that of SR maximization, as N_t increases. This approach maintains a fair rate distribution among users and avoids zero rates for any UE, as already demonstrated in Figs. 4 and 5

Figs. 10 and 11 show that unlike the conventional passive-RIS-based implementation, which fails to achieve any increase

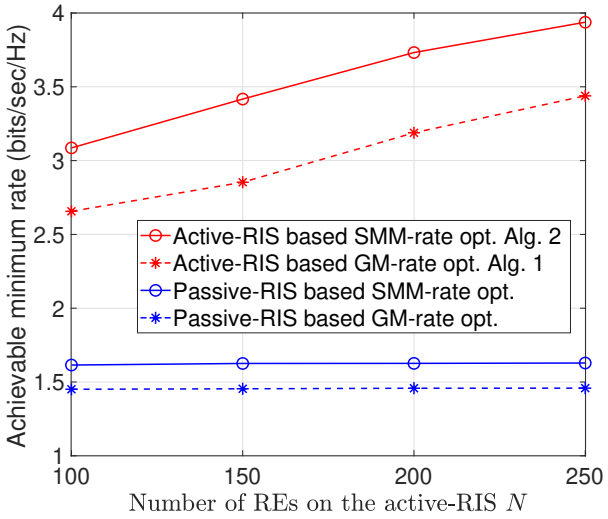

Fig. 10: Achievable MR versus the number of PREs N.

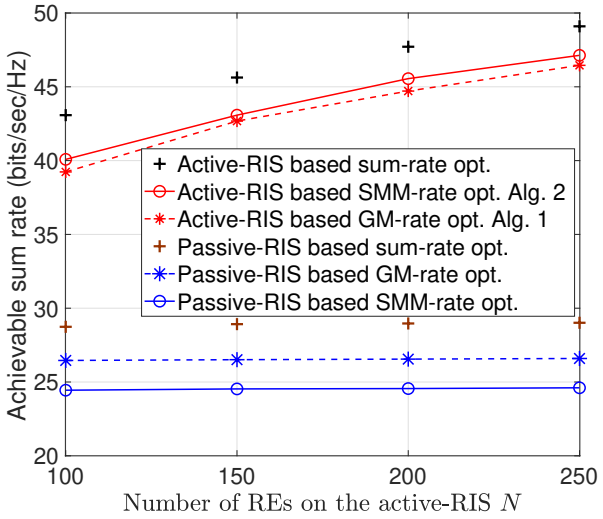

Fig. 11: Achievable SR versus the number of PREs N.

in the achievable MR or SR upon increasing N, our proposed active-RIS based optimization algorithms manage to increase the achievable MR or achievable SR upon increasing N. When initialized by the solution of the active-RIS based GM-rate maximization Algorithm 1, the active-RIS-based SMM-rate optimization Algorithm 2 is capable of further enhancing the MR and SR over a range of values of N. The resultant gain is around 17% in terms of the achievable minimum user-rate and around 2% in terms of the sum rate.

Next, the computational complexity of the proposed algorithms is analysed.

Table III shows that, on average, the GM-rate optimization Algorithm 1 and SMM-rate optimization Algorithm 2 require 38.2 and 58.3 iterations for convergence, respectively. For the SMM-rate optimization Algorithm 2, we include the number of iterations required for its initialization, because it is initialized from the solution of the GM-rate maximization Algorithm 2. The readings are obtained by assuming $N_t = 10$ transmit antennas, $N = 100$ active-PREs, $S = 64$ subcarriers, and $K = 10$ UEs, at $P = 32$ dBm. Notably, both algorithms exhibit scalable complexities and are computationally efficient due to their iterative nature and the evaluation of closed-form expressions.

VI. Conclusions

The potential of an active-RIS-assisted MU MC system in delivering high rates to all users has been investigated. The joint design of the RIS's PREs and the transmit beamformers at the BS has been addressed to enhance the users' individual rates. To overcome the intractability of large-scale computation in the conventional max-min rate optimization, we have proposed two surrogate problems: GM-rate maximization and soft max-min rate optimization. Specifically, we have developed computational solutions that iterate closed-form expressions for gradually enhancing both the PREs and multi-user beamformers for arbitrarily large multi-user networks. Under the same total power-budget, the proposed active-RIS-assisted MU MC system design has approximately doubled the achievable MR or SR compared to the RIS-less or passive-RIS-assisted MU MC system. Moreover, the advantage of our proposed GM-rate and SMM-rate optimization-based designs over the conventional SR-maximization-based design has been demonstrated in terms of providing rate-fairness for all users. The performance of our proposed algorithms can serve as a benchmark for future studies.

Appendix A: Bisection procedure for computing (29) or (58)

Given positive semi-definite matrices Q_s and E_s of size $N \times N$, vectors $b_{k,s} \in \mathbb{C}^N$, $s = 0, \ldots, S$, and $P_1 > 0$, and $P_2 > 0$, consider the following convex problem:

$$\max_{\boldsymbol{x}} \quad f(\boldsymbol{x}) \triangleq -2 \sum_{k=1}^{K} \sum_{s=0}^{S-1} \Re\{\langle b_{k,s}, \boldsymbol{x}_{k,s} \rangle\} + \sum_{k=1}^{K} \sum_{s=0}^{S-1} \boldsymbol{x}_{k,s}^H Q_s \boldsymbol{x}_{k,s} \tag{67a}$$

$$\text{s.t.} \quad \sum_{k=1}^{K} \sum_{s=0}^{S-1} \|\boldsymbol{x}_{k,s}\|^2 \leq P_1, \tag{67b}$$

$$\sum_{k=1}^{K} \sum_{s=0}^{S-1} \boldsymbol{x}_{k,s}^H E_s \boldsymbol{x}_{k,s} \leq P_2. \tag{67c}$$

An obvious solution of (67) is

$$x_{k,s}^{\text{opt}} = (Q_s)^{-1} b_{k,s}, \tag{68}$$

whenever

$$\sum_{k=1}^{K} \sum_{s=0}^{S-1} \| (Q_s)^{-1} b_{k,s} \|^2 \leq P_1 \tag{69}$$

and

$$\sum_{k=1}^{K} \sum_{s=0}^{S-1} (b_{k,s})^H (Q_s)^{-1} E_s (Q_s)^{-1} b_{k,s} \leq P_2. \tag{70}$$

TABLE III: Complexity of GM-rate and SMM-rate optimization algorithms for $N_t = 10$ transmit antennas, $N = 100$ PREs, $S = 64$ subcarriers, and $K = 10$ UEs, at $P = 32$ dBm.

	GM-rate optimization Alg. 1		SMM-rate optimization Alg. 2	
	Beamforming ascent	PREs ascent	Beamforming optimiz.	PREs optimiz.
Computational Complexity	$\mathcal{O}\left(N_t \log_2(N_t) KS\right)$	$\mathcal{O}(N \log_2(N))$	$\mathcal{O}\left(N_t \log_2(N_t) KS\right)$	$\mathcal{O}(N \log_2(N))$
Average # of iterations for convergence	38.2		58.3	
Average computation time per iteration	2.27 sec		2.4 sec	

If (70) is not met, we use bisection to find μ_2 so that

$$\sum_{k=1}^{K}\sum_{s=0}^{S-1}\left(b_{k,s}\right)^H\left(Q_s+\mu_2 E_s\right)^{-1}E_s\left(Q_s+\mu_2 E_s\right)^{-1}b_{k,s} = P_2. \quad (71)$$

Then the solution of (67) is

$$x_{k,s}^{\text{opt}} = \left(Q_s+\mu_2 E_s\right)^{-1} b_{k,s}, \quad (72)$$

whenever

$$\sum_{k=1}^{K}\sum_{s=0}^{S-1}\left\|\left(Q_s+\mu_2 E_s\right)^{-1} b_{k,s}\right\|^2 \le P_1. \quad (73)$$

Analogously, whenever (69) is not met, we use bisection to find μ_1 so that

$$\sum_{k=1}^{K}\sum_{s=0}^{S-1}\left\|\left(Q_s+\mu_1 I_{N_t}\right)^{-1} b_{k,s}\right\|^2 = P_1. \quad (74)$$

The solution of (67) is given by

$$x_{k,s}^{\text{opt}} = \left(Q_s+\mu_1 I_{N_t}\right)^{-1} b_{k,s} \quad (75)$$

if

$$\sum_{k=1}^{K}\sum_{s=0}^{S-1}\left(b_{k,s}\right)^H\left(Q_s+\mu_1 I_{N_t}\right)^{-1}E_s\left(Q_s+\mu_1 I_{N_t}\right)^{-1}b_{k,s} \le P_2. \quad (76)$$

For the remaining case when (71) and (74) are not met, the solution of (67) is

$$x_{k,s}^{\text{opt}} = \left(Q_s+\mu_2 E_s+\mu_1 I_{N_t}\right)^{-1} b_{k,s}, \quad (77)$$

where $\mu_1 > 0$ and $\mu_2 > 0$ are the roots of the nonlinear equations:

$$\sum_{k=1}^{K}\sum_{s=0}^{S-1}\left\|\left(Q_s+\mu_2 E_s+\mu_1 I_{N_t}\right)^{-1} b_{k,s}\right\|^2 = P_1, \quad (78a)$$

$$\sum_{k=1}^{K}\sum_{s=0}^{S-1}\left(b_{k,s}\right)^H\left(Q_s+\mu_2 E_s+\mu_1 I_{N_t}\right)^{-1}E_s \times\left(Q_s+\mu_2 E_s+\mu_1 I_{N_t}\right)^{-1} b_{k,s} = P_2, \quad (78b)$$

which however are computationally intractable. To resolve this issue, we employ a partial Lagrange multiplier method, which aims to find $\lambda_2 > 0$, so that the solution of the problem

$$\min_{\boldsymbol{x}}\ f(\boldsymbol{x}) + \lambda_2\left(\sum_{k=1}^{K}\sum_{s=0}^{S-1}\boldsymbol{x}_{k,s}^H E_s \boldsymbol{x}_{k,s} - P_2\right) \quad \text{s.t.} \quad (67b), \quad (79)$$

satisfies $\sum_{k=1}^{K}\sum_{s=0}^{S-1}\boldsymbol{x}_{k,s}^H E_s \boldsymbol{x}_{k,s} = P_2$. For fixed λ_2, the solution of (79) is given by

$$x_{k,s}(\lambda_2) = \begin{cases} \left(Q_s+\lambda_2 E_s\right)^{-1} b_{k,s} & \text{if } \omega \le P_1 \\ \left(Q_s+\lambda_2 E_s+\lambda_1 I_{N_t}\right)^{-1} b_{k,s} & \text{otherwise,} \end{cases} \quad (80)$$

where

$$\omega = \sum_{k=1}^{K}\sum_{s=0}^{S-1}\left\|\left(Q_s+\lambda_2 E_s\right)^{-1} b_{k,s}\right\|^2,$$

and λ_1 is found by bisection such that $\sum_{k=1}^{K}\sum_{s=0}^{S-1}\left\|\left(Q_s+\lambda_2 E_s+\lambda_1 I_{N_t}\right)^{-1} b_{k,s}\right\|^2 = P_1$. It follows from (76) that $\sum_{k=1}^{K}\sum_{s=0}^{S-1} x_{k,s}^H(0) E_s x_{k,s}(0) > P_2$, while for λ_2 sufficiently large

$$\sum_{k=1}^{K}\sum_{s=0}^{S-1} x_{k,s}^H(\lambda_2) E_s x_{k,s}(\lambda_2) < P_2.$$

We thus start from $\lambda_l = 0$ and λ_u is such that

$$\sum_{k=1}^{K}\sum_{s=0}^{S-1} x_{k,s}^H(\lambda_u) E_s x_{k,s}(\lambda_u) < P_2,$$

and conduct the following innovative bisection procedure.

We set $\lambda_2 = (\lambda_u + \lambda_l)/2$ and solve the problem (79). We stop the procedure if $\sum_{k=1}^{K}\sum_{s=0}^{S-1} x_{k,s}^H(\lambda_2) E_s x_{k,s}(\lambda_2) \approx P_2$. Otherwise, update $\lambda_l \leftarrow \lambda_2$ if $\sum_{k=1}^{K}\sum_{s=0}^{S-1} x_{k,s}^H(\lambda_2)\ E_s x_{k,s}(\lambda_2) > P_2$ or $\lambda_u \leftarrow \lambda_2$ if $\sum_{k=1}^{K}\sum_{s=0}^{S-1} x_{k,s}^H(\lambda_2) E_s x_{k,s}(\lambda_2) < P_2$.

APPENDIX B: PROOF OF INEQUALITY (42)

By Cauchy's inequality, we have

$$\sqrt[S]{\prod_{i=1}^{S}\frac{1}{q_i}} \le \frac{1}{S}\sum_{i=1}^{S}\frac{1}{q_i}$$

$$\Leftrightarrow\quad \ln\left(\sqrt[S]{\prod_{i=1}^{S}\frac{1}{q_i}}\right) \le \ln\left(\frac{1}{S}\sum_{i=1}^{S}\frac{1}{q_i}\right) \quad (81)$$

$$\Leftrightarrow\quad \frac{1}{S}\sum_{i=1}^{S}\ln\frac{1}{q_i} \le \ln\left(\frac{1}{S}\sum_{i=1}^{S}\frac{1}{q_i}\right) \quad (82)$$

$$\Leftrightarrow\quad -\frac{1}{S}\sum_{i=1}^{S}\ln\frac{1}{q_i} \ge -\ln\left(\frac{1}{S}\sum_{i=1}^{S}\frac{1}{q_i}\right). \quad (83)$$

The inequality (42) is obtained from (83) by using

$$q_i \equiv 1 + \frac{|\hbar_{k,i}(\boldsymbol{\upsilon})\mathbf{w}_k(i)|^2}{\sum_{j\in\mathcal{K}\setminus\{k\}}|\hbar_{k,i}(\boldsymbol{\upsilon})\mathbf{w}_j(i)|^2 + \|\bar{g}_{\text{R-k,i}}\boldsymbol{\Upsilon}\|^2\sigma_{\tilde{n}}^2 + \sigma^2}, \quad i = 1,\ldots,S.$$

REFERENCES

[1] M. Di Renzo, A. Zappone, M. Debbah, M.-S. Alouini, C. Yuen, J. de Rosny, and S. Tretyakov, "Smart radio environments empowered by reconfigurable intelligent surfaces: How it works, state of research, and the road ahead," *IEEE J. Sel. Areas Commun.*, vol. 38, pp. 2450–2525, Nov. 2020.

[2] C. Liaskos, S. Nie, A. Tsioliaridou, A. Pitsillides, S. Ioannidis, and I. Akyildiz, "A new wireless communication paradigm through software-controlled metasurfaces," *IEEE Commun. Mag.*, vol. 56, pp. 162–169, Sept. 2018.

[3] C. Pan, H. Ren, K. Wang, J. F. Kolb, M. Elkashlan, M. Chen, M. Di Renzo, Y. Hao, J. Wang, A. L. Swindlehurst, X. You, and L. Hanzo, "Reconfigurable intelligent surfaces for 6G systems: Principles, applications, and research directions," *IEEE Commun. Mag.*, vol. 59, pp. 14–20, June 2021.

[4] C. Huang, A. Zappone, G. C. Alexandropoulos, M. Debbah, and C. Yuen, "Reconfigurable intelligent surfaces for energy efficiency in wireless communication," *IEEE Trans. Wirel. Commun.*, vol. 18, pp. 4157–4170, Aug. 2019.

[5] C. Pan, H. Ren, K. Wang, W. Xu, M. Elkashlan, A. Nallanathan, and L. Hanzo, "Multicell MIMO communications relying on intelligent reflecting surface," *IEEE Trans Wirel. Commun.*, vol. 19, pp. 5218–5233, Aug. 2020.

[6] H. Xie, J. Xu, and Y.-F. Liu, "Max-min fairness in IRS-aided multi-cell MISO systems with joint transmit and reflective beamforming," *IEEE Trans. Wirel. Commun.*, vol. 20, pp. 1379–1393, Feb. 2021.

[7] H. Yu, H. D. Tuan, A. A. Nasir, T. Q. Duong, and H. V. Poor, "Joint design of reconfigurable intelligent surfaces and transmit beamforming under proper and improper Gaussian signaling," *IEEE J. Sel. Areas Commun.*, vol. 38, pp. 2589–2603, Nov. 2020.

[8] C. Pan, G. Zhou, K. Zhi, S. Hong, T. Wu, Y. Pan, H. Ren, M. Di Renzo, A. L. Swindlehurst, R. Zhang and A. Y. Zhang , "An overview of signal processing techniques for RIS/IRS-aided wireless systems," *IEEE J. Selec. Topics Signal Process.*, vol. 16, pp. 883–917, May 2022.

[9] J. Qiu, J. Yu, A. Dong, and K. Yu, "Joint beamforming for IRS-aided multi-cell MISO system: Sum rate maximization and SINR balancing," *IEEE Trans. Wirel. Commun.*, vol. 21, pp. 7536–7549, Sept. 2022.

[10] H. Yu, H. D. Tuan, E. Dutkiewicz, H. V. Poor, and L. Hanzo, "Maximizing the geometric mean of user-rates to improve rate-fairness: Proper vs. improper Gaussian signaling," *IEEE Trans. Wirel. Commun.*, vol. 21, pp. 295–309, Jan. 2022.

[11] A. A. Nasir, H. D. Tuan, E. Dutkiewicz, H. V. Poor, and L. Hanzo, "Low-resolution RIS-aided multiuser MIMO signaling," *IEEE Trans. Commun.*, vol. 70, pp. 6517–6531, Oct. 2022.

[12] G. Zhou, C. Pan, H. Ren, K. Wang, W. Xu, and A. Nallanathan, "Intelligent reflecting surface aided multigroup multicast MISO communication systems," *IEEE Trans. Signal Process.*, vol. 68, pp. 3236–3251, Apr. 2020.

[13] O. Ozdogan, E. Bjornson, and E. G. Larsson, "Intelligent reflecting surfaces: Physics, propagation, and pathloss modeling," *IEEE Wirel. Commun. Lett.*, vol. 9, pp. 581–585, May 2020.

[14] R. Long, Y.-C. Liang, Y. Pei, and E. G. Larsson, "Active reconfigurable intelligent surface-aided wireless communications," *IEEE Trans. Wirel. Commun.*, vol. 20, pp. 4962–4975, Aug. 2021.

[15] Z. Zhang, L. Dai, X. Chen, C. Liu, F. Yang, R. Schober, and H. V. Poor, "Active RIS vs. passive RIS: Which will prevail in 6G?," *IEEE Trans. Commun.*, vol. 71, pp. 1707–1725, Mar. 2023.

[16] H. Niu, Z. Lin, K. An, J. Wang, G. Zheng, N. Al-Dhahir, and K.-K. Wong, "Active RIS assisted rate-splitting multiple access network: Spectral and energy efficiency tradeoff," *IEEE J. Sel. Areas Commun.*, vol. 41, pp. 1452–1467, May 2023.

[17] Y. Ma, M. Li, Y. Liu, Q. Wu, and Q. Liu, "Active reconfigurable intelligent surface for energy efficiency in MU-MISO systems," *IEEE Trans. Veh. Technol.*, vol. 72, pp. 4103–4107, Mar. 2023.

[18] A. Goldsmith, *Wireless Commununications*. New York, NY, USA: Cambridge University Press, 2005.

[19] Y. Yang, B. Zheng, S. Zhang, and R. Zhang, "Intelligent reflecting surface meets OFDM: Protocol design and rate maximization," *IEEE Trans. Commun.*, vol. 68, pp. 4522–4535, July 2020.

[20] K. Feng, Y. Chen, Y. Han, X. Li, and S. Jin, "Passive beamforming design for reconfigurable intelligent surface-aided OFDM: A fractional programming based approach," in *Proc. IEEE Veh. Techn. Conf. (VTC)*, pp. 1–6, 2021.

[21] T. Zhang, S. Wang, Y. Zhuang, C. You, M. Wen, and Y.-C. Wu, "Reconfigurable intelligent surface assisted OFDM relaying: Subcarrier matching with balanced SNR," *IEEE Trans. Veh. Technol.*, vol. 72, pp. 2216–2230, Feb. 2023.

[22] S. Lin, B. Zheng, G. C. Alexandropoulos, M. Wen, F. Chen, and S. sMumtaz, "Adaptive transmission for reconfigurable intelligent surface-assisted OFDM wireless communications," *IEEE J. Sel. Areas Commun.*, vol. 38, no. 11, pp. 2653–2665, 2020.

[23] B. Zheng, C. You, and R. Zhang, "Intelligent reflecting surface assisted multi-user OFDMA: Channel estimation and training design," *IEEE Trans. Wirel. Commun.*, vol. 19, pp. 8315–8329, Dec. 2020.

[24] W. R. Ghanem, V. Jamali, and R. Schober, "Joint beamforming and phase shift optimization for multicell IRS-aided OFDMA-URLLC systems," in *Proc. IEEE Wirel. Commun. Netw. Conf. (WCNC)*, pp. 1–7, 2021.

[25] L. Wei, C. Huang, G. C. Alexandropoulos, C. Yuen, Z. Zhang, and M. Debbah, "Channel estimation for RIS-empowered multi-user MISO wireless communications," *IEEE Tran. Commun.*, vol. 69, pp. 4144–4157, June 2021.

[26] W. Hao, G. Sun, M. Zeng, Z. Chu, Z. Zhu, O. A. Dobre and P. Xiao, "Robust design for intelligent reflecting surface-assisted MIMO-OFDMA, Terahertz IoT networks," *IEEE Int. Things J.*, vol. 8, pp. 13052–13064, Aug. 2021.

[27] H. Li, W. Cai, Y. Liu, M. Li, Q. Liu and Q. Wu, "Intelligent reflecting surface enhanced wideband MIMO-OFDM communications: From practical model to reflection optimization," *IEEE Trans. Commun.*, vol. 69, pp. 4807–4820, July 2021.

[28] H. Yu, H. D. Tuan, A. A. Nasir, E. Dutkiewicz, and L. Hanzo, "Rate-fairness-aware low resolution ris-aided multi-user ofdm beamforming," *IEEE Trans. Veh. Tech.*, vol. 73, pp. 2401–2415, Feb. 2024.

[29] A. A. Nasir, H. D. Tuan, E. Dutkiewicz, H. V. Poor, and L. Hanzo, "Relay-aided multi-user OFDM relying on joint wireless power transfer and self-interference recycling," *IEEE Trans. Commun.*, vol. 70, pp. 291–305, Jan. 2022.

[30] J. Zhang, Z. Li, and Z. Zhang, "Wideband active RISs: Architeccture, modeling, and beamforming design," *IEEE Commun. Lett.*, vol. 27, pp. 1899–1903, July 2023.

[31] W. Yu and R. Lui, "Dual method for nonconvex spectrum optimization of multicarrier systems," *IEEE Trans. Commun.*, vol. 54, pp. 1310–1322, July 2006.

[32] J. Papandriopoulos and J. S. Evans, "SCALE: a low-complexity distributed protocol for spectrum balancing in multi-user DSL networks," *IEEE Trans. Info. Theory*, vol. 55, pp. 3711–3724, Aug. 2009.

[33] H. H. M. Tam, H. D. Tuan, and D. T. Ngo, "Successive convex quadratic programming for quality-of-service management in full-duplex MU-MIMO multicell networks," *IEEE Trans. Commun.*, vol. 64, pp. 2340–2353, June 2016.

[34] H. Tuy, *Convex Analysis and Global Optimization (second edition)*. Springer International, 2017.

[35] H. Dong, C. Ji, L. Zhou, J. Dai, and Z. Ye, "Sparse channel estimation with surface clustering for IRS-assisted OFDM systems," *IEEE Trans. Commun.*, vol. 71, pp. 1083–1095, Feb. 2023.

[36] Y. Lin, S. Jin, M. Matthaiou, and X. You, "Channel estimation and user localization for IRS-assisted MIMO-OFDM systems," *IEEE Trans. Wirel. Commun.*, vol. 21, pp. 2320–2335, Apr. 2022.

[37] S. Yang, W. Lyu, Y. Xiu, Z. Zhang, and C. Yuen, "Active 3D double-RIS-aided multi-user communications: Two-timescale-based separate channel estimation via Bayesian learning," *IEEE Trans. Commun.*, vol. 71, pp. 3605–3620, June 2023.

[38] J.-F. Bousquet, S. Magierowski, and G. G. Messier, "A 4-GHz active scatterer in 130-nm CMOS for phase sweep amplify-and-forward," *IEEE Trans Circ. Syst. I*, vol. 59, pp. 529–540, Mar. 2012.

[39] K. Zhi, C. Pan, H. Ren, K. K. Chai, and M. Elkashlan, "Active RIS versus passive RIS: Which is superior with the same power budget?," *IEEE Commun. Lett.*, vol. 26, pp. 1150–1154, May 2022.

[40] A. H. Phan, H. D. Tuan, H. H. Kha, and H. H. Nguyen, "Beamforming optimization in multi-user amplify-and-forward wireless relay networks," *IEEE Trans. Wirel. Coomun.*, vol. 11, pp. 1510–1520, Apr. 2012.

[41] S. W. Ellingson, "Path loss in reconfigurable intelligent surface-enabled channels," in *IEEE Proc. PIMRC*, pp. 829–835, 2021.

Hoang Duong Tuan received the Diploma (Hons.) and Ph.D. degrees in applied mathematics from Odessa State University, Ukraine, in 1987 and 1991, respectively. He spent nine academic years in Japan as an Assistant Professor in the Department of Electronic-Mechanical Engineering, Nagoya University, from 1994 to 1999, and then as an Associate Professor in the Department of Electrical and Computer Engineering, Toyota Technological Institute, Nagoya, from 1999 to 2003. He was a Professor with the School of Electrical Engineering and Telecommunications, University of New South Wales, from 2003 to 2011. He is currently a Professor with the School of Electrical and Data Engineering, University of Technology Sydney. He has been involved in research with the areas of optimization, control, signal processing, wireless communication, and biomedical engineering for more than 30 years.

Ali Arshad Nasir received his Ph.D. degree in telecommunications engineering from the Australian National University (ANU), Australia, in 2013. From 2012 to 2015, he worked as a Research Fellow at ANU. From 2015 to 2016, he was an Assistant Professor in the School of Electrical Engineering and Computer Science (SEECS) at the National University of Sciences and Technology (NUST), Pakistan. He joined the Department of Electrical Engineering at King Fahd University of Petroleum and Minerals (KFUPM), Dhahran, Saudi Arabia, in 2016, where he is currently working as an Associate Professor. His research interests are in the area of signal processing in wireless communication systems. He is an Associate Editor for IEEE Communications Letters.

Eryk Dutkiewicz (SM'17) received his B.E. degree in Electrical and Electronic Engineering from the University of Adelaide in 1988, his M.Sc. degree in Applied Mathematics from the University of Adelaide in 1992 and his PhD in Telecommunications from the University of Wollongong in 1996. His industry experience includes management of the Wireless Research Laboratory at Motorola in early 2000's. Prof. Dutkiewicz is currently Associate Dean International in the Faculty of Engineering and IT at University of Technology Sydney, Australia. He is a Senior Member of IEEE. He also holds a professorial appointment at Hokkaido University in Japan. His current research interests cover 5G/6G and IoT networks.

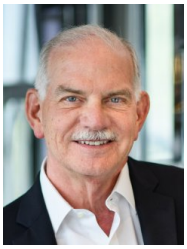

H. Vincent Poor (S'72, M'77, SM'82, F'87) received the Ph.D. degree in EECS from Princeton University in 1977. From 1977 until 1990, he was on the faculty of the University of Illinois at Urbana-Champaign. Since 1990 he has been on the faculty at Princeton, where he is currently the Michael Henry Strater University Professor. During 2006 to 2016, he served as the dean of Princeton's School of Engineering and Applied Science. He has also held visiting appointments at several other universities, including most recently at Berkeley and Cambridge. His research interests are in the areas of information theory, machine learning and network science, and their applications in wireless networks, energy systems and related fields. Among his publications in these areas is the recent book *Machine Learning and Wireless Communications* (Cambridge University Press, 2022). Dr. Poor is a member of the National Academy of Engineering and the National Academy of Sciences and is a foreign member of the Royal Society and other national and international academies. He received the IEEE Alexander Graham Bell Medal in 2017.

Lajos Hanzo (F'04) received Honorary Doctorates from the Technical University of Budapest (2009) and Edinburgh University (2015). He is a Foreign Member of the Hungarian Science-Academy, Fellow of the Royal Academy of Engineering (FREng), of the IET, of EURASIP and holds the IEEE Eric Sumner Technical Field Award. For further details please see http://www-mobile.ecs.soton.ac.uk, https://en.wikipedia.org/wiki/Lajos_Hanzo